

# T3C: Test-Time Tensor Compression with Consistency Guarantees

Ismail Lamaakal<sup>1</sup> Chaymae Yahyati<sup>1</sup> Yassine Maleh<sup>2</sup> Khalid El Makkaoui<sup>1</sup> Ibrahim Ouahbi<sup>1</sup>

## Abstract

We present **T3C**, a train-once, test-time *budget-conditioned* compression framework that exposes rank and precision as a controllable deployment knob. T3C combines elastic tensor factorization (maintained up to a maximal rank) with rank-tied mixed-precision quantization and a lightweight controller that maps a latency/energy/size budget token to per-layer rank/bit assignments; the policy snaps to hardware-aligned profiles and is monotone in the budget. A fast, layerwise *consistency certificate*, computed from spectral proxies and activation statistics, upper-bounds logit drift and regularizes training, yielding a practical reliability signal with negligible overhead. On ImageNet-1k, T3C shifts the vision Pareto frontier: for *ResNet-50* at matched accuracy ( $\leq 0.5\%$  drop), p50 latency is **1.18 ms** with a **38 MB** model, outperforming PTQ-8b (1.44 ms, 88 MB); for *ViT-B/16*, T3C reaches **2.30 ms** p50 with **59 MB**, improving over strong PTQ/QAT baselines. A single T3C checkpoint therefore provides predictable, certificate-backed accuracy-latency-size trade-offs on demand across devices.

## 1. Introduction

Modern ML systems increasingly run across a spectrum of deployment targets—shared cloud accelerators under variable multiplexing (Yu & Chowdhury, 2020), edge deployments subject to thermal throttling (Zhou et al., 2022), and battery-powered platforms where dynamic voltage/frequency scaling can reshape latency/throughput behavior (Han et al., 2025). In these settings, the effective compute and memory budgets are not static; they fluctuate with co-tenancy (Yu & Chowdhury, 2020), heat (Zhou et al., 2022), and background workloads (Gujarati et al., 2020). Yet most compression pipelines in practice are compiled for

a single operating point: quantization-only exports at one bit-width (Jacob et al., 2017; Esser et al., 2020), pruning-only checkpoints with a fixed sparsity (Han et al., 2015a; Gale et al., 2019), or factorized models frozen at a particular rank (Jaderberg et al., 2014; Denton et al., 2014; Lebedev et al., 2015). When the runtime envelope shifts even modestly, these static exports may miss latency SLOs, violate memory caps, or shed more accuracy than expected—forcing operators to keep multiple model variants and ad hoc routing logic that complicate A/B rollouts and on-call playbooks (Crankshaw et al., 2017; Gujarati et al., 2020).

A natural response is to assemble menus of checkpoints (e.g., 4/6/8-bit; 30/50/80% sparsity; several low-rank truncations) and switch among them at inference. However, the combinatorics grow quickly, compatibility across devices is uneven, and compiler/kernel autotuning can introduce substantial sensitivity to backend choices (Chen et al., 2018; Zheng et al., 2020). Furthermore, each checkpoint typically requires separate training or post-training calibration (Nagel et al., 2020; Li et al., 2021), inflating cost and slowing iteration. What practitioners want instead is a *single* model that can be steered *at test time* to a target latency/size/energy point with predictable accuracy behavior, as pursued by train-once / specialize-many paradigms (Yu et al., 2019; Yu & Huang, 2019; Cai et al., 2020).

Prior lines of work each address parts of this need but leave key gaps. Post-training quantization (PTQ) is fast to produce (Nagel et al., 2020; Li et al., 2021) but can be fragile when calibration conditions shift (Yuan et al., 2023); for large models, heavy-tailed activation outliers are a known failure mode that motivates specialized PTQ treatments (Xiao et al., 2023; Dettmers et al., 2022). Quantization-aware training (QAT) improves stability (Jacob et al., 2017; Esser et al., 2020) but still locks the export to a fixed precision. Magnitude and movement pruning reduce compute (Han et al., 2015a; Sanh et al., 2020) but often rely on sparse kernels whose realized speedups can vary by engine/hardware, motivating methods that explicitly target speedup constraints (Frantar & Alistarh, 2022). Low-rank methods trade FLOPs for accuracy cleanly (Jaderberg et al., 2014; Denton et al., 2014; Lebedev et al., 2015), yet selecting ranks is typically an offline choice and the resulting approximation error can interact nontrivially with mixed precision; factorization choices also appear in Transformer parameter-sharing de-

<sup>1</sup> Multidisciplinary Faculty of Nador, Mohammed Premier University, Oujda 60000, Morocco <sup>2</sup> Laboratory LaSTI, ENSAK, Sultan Moulay Slimane University, Khouribga 54000, Morocco. Correspondence to: Ismail Lamaakal <ismail.lamaakal@ieee.org>.

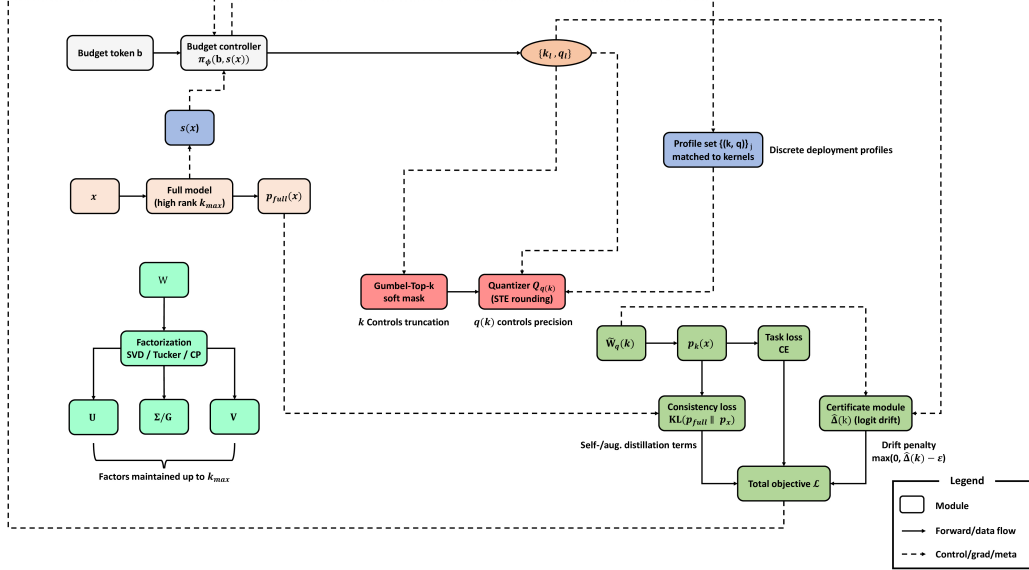


**Figure 1. Detailed T3C pipeline (train once, control at test time).** Given an input  $x$ , the **full (teacher) model** evaluated at high rank  $k_{\max}$  produces **teacher logits/distribution**  $p_{\text{full}}(x)$  and an optional **input summary**  $s(x)$ . A **budget token**  $b$  (e.g., latency/energy/size target) together with  $s(x)$  is consumed by the **budget controller**  $\pi_{\phi}(b, s(x))$ , which outputs per-layer **rank and precision assignments**  $\{k_{\ell}, q_{\ell}\}$ . In parallel, each layer’s weight tensor  $W$  is stored in an **elastic factorization** (SVD/Tucker/CP) maintained up to  $k_{\max}$ . A differentiable **Gumbel-Top- $k$  soft mask** activates the first  $k_{\ell}$  spectral/tensor components (**rank control**), and a **rank-tied mixed-precision quantizer**  $Q_{q_{\ell}}$  with STE rounding applies  $q_{\ell}$ -bit quantization (**bit-width control**) to form compressed weights  $\tilde{W}_q(k)$ . The recomposed operator yields compressed predictions  $p_k(x)$ , trained using (i) the **task loss** (CE) and (ii) **consistency/self-distillation** via  $\text{KL}(p_{\text{full}} \parallel p_k)$  (optionally also under light augmentations). A **certificate module** estimates the **logit-drift**  $\hat{\Delta}(k)$  and contributes a drift-penalty term (e.g.,  $\max(0, \hat{\Delta}(k) - \epsilon)$ ) to the total objective  $\mathcal{L}$ . For deployment, continuous  $(k_{\ell}, q_{\ell})$  choices are **snapped to a discrete profile set**  $\{(k, q)\}_j$  matched to hardware-efficient kernels, enabling predictable runtime behavior. Solid arrows denote forward/data flow; dashed arrows denote control/meta or gradient pathways.

signs (Lan et al., 2020). Finally, “dynamic” networks (early exits, adaptive routing/width/depth) require architectural changes and can be harder to integrate into standard serving stacks (Teerapittayanan et al., 2016; Wang et al., 2018b; Graves, 2016; Hou et al., 2020).

From an operational perspective, three desiderata emerge. *First*, deployments need **monotone trade-offs**: tightening a budget should never *increase* realized latency/size, and relaxing it should not *decrease* accuracy. *Second*, teams need **tail-risk control**: p90/p99 latency and violation rates must remain stable despite kernel choices, cache residency, and allocator jitter (Gujarati et al., 2020). *Third*, any solution must be **device aware**: cost models must couple compute and memory traffic so that a single artifact travels across compute-bound servers and memory-bound edge hardware without per-target retraining (Williams et al., 2009; Chen et al., 2018). These requirements imply an interface that is continuous during training (to learn robust behaviors) yet discrete at export (to align with hardware-efficient kernels), and they call for principled *certificates* that summarize how much accuracy may degrade when budgets change at test time, drawing inspiration from certification methodologies that produce explicit, checkable bounds (Weng et al., 2018;

Cohen et al., 2019).

**In this paper, we introduce T3C**, a budget-conditioned, train-once/test-time compression framework that turns compression from an offline decision into an online control. T3C couples elastic tensorization (SVD/Tucker/CP up to a maximal rank) with per-factor mixed-precision quantization, and uses a lightweight policy to map a structured budget token (latency, bytes, optional energy) to layerwise rank/bit assignments. A profile snapper projects these assignments onto a small lattice of hardware-aligned kernels, ensuring stable and fast execution, while a calibrated *consistency certificate* aggregates layerwise residual norms and activation statistics to upper-bound logit drift. Our contributions are: (1) a *budget-conditioned* parameterization that exposes a continuous rank-precision dial during training but compiles to discrete, device-ready profiles; (2) a *device-aware controller* that consumes tuple budget tokens and optimizes a hybrid compute/bytes proxy for portability across cloud and edge; (3) a fast *certificate* that regularizes training and exports per-profile risk summaries; and (4) an extensive empirical study showing monotone, hardware-aligned accuracy-latency-size trade-offs from a *single* checkpoint, with reduced tail risk relative to strong quantization, pruning, and

low-rank baselines.

The remainder of this paper is organized as follows: Section 2 reviews related work and sets notation. Section 3 presents the elastic factorization, differentiable truncation/quantization, the budgeted controller, and the overall training objective. Section 4 states the certificate, discusses its computation and deployment complexity. Section 5 describes the experimental setup and baselines. Section 6 reports results across vision and language, also covers limitations and broader impact. Section 7 concludes the paper and highlights future directions.

## 2. Related Work and Preliminaries

**Quantization.** Post-training quantization (PTQ) and quantization-aware training (QAT) reduce precision to shrink size and improve latency, with QAT often improving stability at low bit-widths (Jacob et al., 2017; Esser et al., 2020). Mixed-precision methods allocate bit-widths per layer to improve accuracy–efficiency trade-offs under hardware constraints (Dong et al., 2020). Recent PTQ advances improve robustness via calibration/reconstruction and better rounding decisions (Nagel et al., 2020; Li et al., 2021; Wei et al., 2022), while data-free / distillation-style approaches reduce reliance on original calibration data (Xu et al., 2020; Li et al., 2020). Despite progress, most pipelines still emit a *single* fixed-precision checkpoint, providing limited control at test time and no actionable bound on degradation (see App. A).

**Pruning and sparsity.** Unstructured pruning can reach high sparsity (Han et al., 2015a; Sanh et al., 2020), but realized speedups depend strongly on sparse-kernel availability and backend details (Gale et al., 2019). In contrast, structured sparsity patterns (e.g.,  $N : M$ ) aim for more reliable acceleration on supported hardware (Zhou et al., 2021), and recent work targets pruning with explicit speedup guarantees (Frantar & Alistarh, 2022). Channel/structured pruning can yield predictable latency reductions but often requires careful retraining or automated schedules (Liu et al., 2017; He et al., 2018). Dynamic inference and early exiting adapt compute per input (Teerapittayanon et al., 2016; Wang et al., 2018b) but complicate deployment guarantees. Across these lines, operating points are typically hard-coded at export, and guarantees on output drift remain uncommon.

**Low-rank and LoRA-style methods.** Matrix/tensor factorization (e.g., low-rank approximations, Tucker/CP decompositions) compresses layers by trading rank for compute/accuracy (Denton et al., 2014; Jaderberg et al., 2014; Lebedev et al., 2014; Kim et al., 2015). Low-rank adaptation modules such as LoRA reduce trainable parameters for fine-tuning (Hu et al., 2022), and follow-ups adapt or

redistribute rank/budget during training (Zhang et al., 2023; Valipour et al., 2023). However, rank is still commonly treated as an offline/export-time choice in many compression pipelines, and switching ranks can require re-export and invalidate kernel assumptions; joint rank–bit allocation and end-to-end *shared-parameter* training across many  $k$  remain relatively under-explored.

**Certified compression and robustness bounds.** Sensitivity analysis and Lipschitz/relaxation-based certificates bound output changes under perturbations (Weng et al., 2018), including certificates under *weight* perturbations (Weng et al., 2020). Interval bound propagation offers scalable certified training/verification pipelines (Gowal et al., 2018). For quantized and efficient deployments, integer-arithmetic-only certified robustness has also been studied (Lin et al., 2021). Existing bounds can be conservative or computationally heavy, limiting practical use; they also seldom connect certificates to a deployable controller that enforces budget monotonicity. We instead provide a fast, calibration-based certificate aligned with an actionable budget policy.

### 2.1. Preliminaries

We consider a feed-forward network with layers  $\{\ell = 1, \dots, L\}$  and weights  $W_\ell$ . Given input  $x$ , the full model yields logits  $z = f(x)$ ; under a budget profile, the compressed model yields  $\tilde{z} = \tilde{f}_k(x)$ .

**Elastic factorization.** Dense layers use an SVD factorization up to rank  $k_{\max}$ , with trainable factors  $(U_\ell, \Sigma_\ell, V_\ell)$ :

$$W_\ell \approx \underbrace{U_{\ell,k} \Sigma_{\ell,k} V_{\ell,k}^\top}_{\text{top-}k \text{ reconstruction}}, \quad k \in [k_{\min}, k_{\max}]. \quad (1)$$

Convolutional/attention tensors use Tucker-2 or CP analogues; attention heads can share budgets across projections. A differentiable top- $k$  mask selects active singulars/factors.

**Mixed-precision quantization.** Each active factor (or channel group) is quantized by a bit-width  $q(k)$  tied to the chosen rank, using a straight-through (STE) quantizer  $Q_{q(k)}(\cdot)$ :

$$\tilde{W}_\ell(k) = Q_{q(k)}(U_{\ell,k} \Sigma_{\ell,k} V_{\ell,k}^\top). \quad (2)$$

**Budget, cost, and certificate.** A controller  $\pi_\phi$  maps a budget token  $b$  (e.g., latency/energy/size target) and optional summary  $s(x)$  to per-layer  $(k_\ell, q_\ell)$ . Cost proxies include FLOPs and bytes moved; measured latency/energy are used for profile selection. We summarize the logit drift via a certificate  $\hat{\Delta}(k)$  computed from spectral proxies and activation statistics (details in Sec. 4); at export, the model ships with discrete, hardware-aligned profiles  $\{(k_\ell, q_\ell)\}_j$  and their certificate reports. Extra notation and identities are deferred to Appendix B.

### 3. Method

#### 3.1. Elastic reparameterization

We represent each dense weight matrix  $W \in \mathbb{R}^{m \times n}$  with an elastic, factorized parameterization that supports variable test-time ranks. We maintain the top- $k_{\max}$  singular components and learn a differentiable top- $k$  mask over the spectrum. For a chosen rank  $k \in \{k_{\min}, \dots, k_{\max}\}$ , the effective weight used in the forward pass is

$$\tilde{W}(k) = U_{:,1k} (\Sigma_{1k,1k} \odot M_k) V_{:,1k}^{\top}, \quad (3)$$

where  $U, \Sigma, V$  are SVD factors up to  $k_{\max}$ , and  $M_k \in [0, 1]^{k \times k}$  is a (relaxed during training) diagonal mask selecting active singular values. To couple mixed precision with rank, we quantize factors using a rank-dependent bit-allocation  $q(k)$ . The quantized forward operator is

$$\tilde{W}_q(k) = Q_{q(k)}(U_{:,1k}) \left( Q_{q(k)}(\Sigma_{1k,1k} \odot M_k) \right) Q_{q(k)}(V_{:,1k})^{\top}, \quad (4)$$

where  $Q_q$  applies per-tensor uniform affine quantization with  $q$  bits and learnable scales/zero-points; gradients use straight-through estimators (details in App. B).

For convolutional kernels, we employ Tucker-2 (channel-only) or CP factorization. A kernel  $W \in \mathbb{R}^{C_{\text{out}} \times C_{\text{in}} \times h \times w}$  is decomposed as  $U_{\text{out}} \in \mathbb{R}^{C_{\text{out}} \times r_o}$ , core  $G \in \mathbb{R}^{r_o \times r_i \times h \times w}$ , and  $U_{\text{in}} \in \mathbb{R}^{C_{\text{in}} \times r_i}$ . Budgeted ranks  $(r_o, r_i)$  are produced by the controller in Sec. 3.3 via a monotone schedule  $k \mapsto (r_o(k), r_i(k))$ . In multi-head attention, we share one budget across  $\{W_Q, W_K, W_V, W_O\}$  within a block to avoid head imbalance; per-matrix ranks are split from  $k$  using fixed ratios for compilation simplicity. Mixed precision follows the same rule: each factor receives  $q(k)$  bits, optionally with per-factor offsets (e.g.,  $q_U = q(k) + 1$ ,  $q_G = q(k)$ ,  $q_V = q(k) + 1$ ).

#### 3.2. Differentiable truncation and quantization

We relax the discrete top- $k$  selection with a Gumbel-Top- $k$  mask over singular values or tensor factors. Each spectral element  $s_i$  receives a temperature-controlled logistic score, producing a soft mask  $\hat{m}_i \in [0, 1]$  that approaches a hard keep/drop as the temperature anneals. During the forward pass we multiply  $\Sigma$  (or core slices) by  $\text{diag}(\hat{m}_{1:k_{\max}})$ . Quantization uses uniform bins with learned scales and straight-through rounding so gradients flow through  $Q_q$ . We randomly sample a rank  $k \sim \pi_{\phi}(b)$  each iteration (Sec. 3.3), which stochastically trains the model across the entire range  $k \in [k_{\min}, k_{\max}]$  and avoids train-deploy mismatch.

#### 3.3. Budget-conditioned controller

We control per-layer ranks and bit-widths with a lightweight policy conditioned on a budget token and, optionally, a compact input summary. Let  $b \in \mathbb{R}^{d_b}$  encode the deployment

objective (e.g., target latency/energy/size as indices or embeddings) and let  $s(x) \in \mathbb{R}^{d_s}$  be a low-dimensional statistic (e.g., pooled activations). A shared MLP outputs layerwise rank/bit proposals projected onto a small hardware-friendly discrete set. We write

$$\{k_{\ell}, q_{\ell}\}_{\ell=1}^L = \pi_{\phi}(b, s(x)). \quad (5)$$

Training uses either a differentiable relaxation (soft masks with straight-through discretization) or a policy-gradient objective that treats the negative training loss plus a budget satisfaction reward as the return. To ensure deployability,  $\{k_{\ell}, q_{\ell}\}$  are snapped to a calibrated profile set matched to available kernels, monotone in  $b$  so larger budgets never yield smaller ranks or bits. We employ a curriculum: (i) global-budget only (no  $s(x)$ ) for stability, (ii) tighter budgets, and (iii) optional input-aware refinements on a subset of layers.

#### 3.4. Training objective

The total loss combines task performance, self-distillation between the full and compressed views, augmentation consistency, a certificate penalty that caps predicted logit drift, and a differentiable budget cost:

$$\begin{aligned} \mathcal{L} = & \underbrace{\text{CE}(f_{\text{full}}(x), y)}_{\text{task}} + \lambda_{\text{SD}} \underbrace{\text{KL}(p_{\text{full}}(x) \parallel p_k(x))}_{\text{self distill}} \\ & + \lambda_{\text{AUG}} \underbrace{\mathbb{E}_{\tilde{x}} \text{KL}(p_{\text{full}}(\tilde{x}) \parallel p_k(\tilde{x}))}_{\text{aug. consistency}} \\ & + \lambda_{\text{CERT}} \underbrace{\max(0, \hat{\Delta}(k) - \epsilon)}_{\text{drift cap}} + \lambda_{\text{BUD}} \underbrace{\text{Cost}(k, b)}_{\text{budget}}. \end{aligned} \quad (6)$$

The cross-entropy term trains the full-capacity view (evaluated at  $k = k_{\max}$  or a high-rank proxy) to solve the task. The self-distillation term aligns the compressed prediction  $p_k$  to the full model’s distribution  $p_{\text{full}}$  on the same inputs, stabilizing accuracy across ranks. The augmentation-consistency term repeats the alignment on perturbed inputs  $\tilde{x}$  (e.g., weak augmentations) to prevent rank-specific overfitting. The certification penalty uses a fast, layerwise spectral-norm proxy to compute a predicted logit-shift  $\hat{\Delta}(k)$ ; if this exceeds a tolerance  $\epsilon$ , the controller is nudged toward safer profiles (Sec. 4). Finally, the budget term penalizes expected compute/memory/latency under the sampled profile using a calibrated proxy combining FLOPs, bytes moved, and device-specific latency tables. Schedules and proxy definitions appear in App. B.

## 4. Consistency Certificate and Deployment Complexity

### 4.1. Bound statement

We provide a certificate that upper-bounds the change of logits when replacing each layer weight  $W_\ell$  with its compressed counterpart  $\tilde{W}_\ell(k)$  produced by our method (see Figure 2). Let  $f(x)$  denote the full model and  $\tilde{f}_k(x)$  the compressed model at budget knob  $k$ . Let  $\delta z(x; k) = \tilde{f}_k(x) - f(x)$  be the logit difference. For each layer  $\ell$ , define a spectral-norm proxy  $\hat{L}_\ell$  that bounds the local Lipschitz factor of the sub-network from the layer output  $h_\ell$  to the logits (estimated via power iterations with normalization) (see App. C for more details). Let  $\Delta W_\ell(k) = W_\ell - \tilde{W}_\ell(k)$  and  $a_{\ell-1}$  be the input activation to layer  $\ell$ . Then:

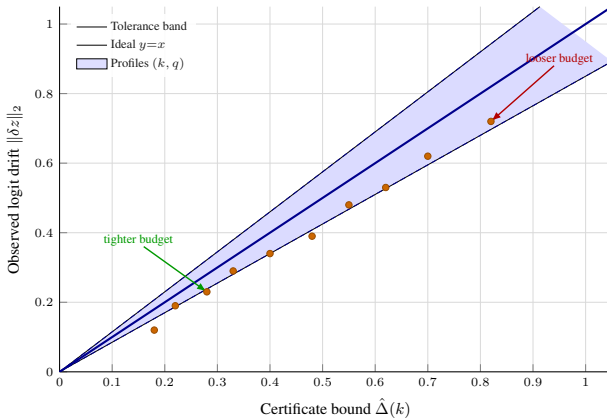


Figure 2. Certificate bound  $\hat{\Delta}(k)$  versus observed logit drift  $\|\delta z\|_2$  across discrete profiles  $(k, q)$ . The shaded region marks a tolerance band around  $y=x$ ; dashed lines show its boundaries. Arrows and labels are positioned in axis coordinates and point to representative profiles.

**Proposition 4.1** (Layerwise truncation certificate). *For ReLU/ GELU networks with standard residual blocks and normalization, and for any input  $x$  in a calibration set  $\mathcal{C}$ , the logit deviation satisfies*

$$\|\delta z(x; k)\|_2 \leq \sum_{\ell=1}^L \hat{L}_\ell \|\Delta W_\ell(k)\|_2 \|a_{\ell-1}(x)\|_2. \quad (7)$$

Moreover, using calibration statistics  $\alpha_\ell = \sqrt{\mathbb{E}_{x \in \mathcal{C}} \|a_{\ell-1}(x)\|_2^2}$ , the expected logit deviation is bounded by

$$\left( \mathbb{E}_{x \in \mathcal{C}} \|\delta z(x; k)\|_2^2 \right)^{1/2} \leq \sum_{\ell=1}^L \hat{L}_\ell \|\Delta W_\ell(k)\|_2 \alpha_\ell. \quad (8)$$

The forward perturbation induced by  $\Delta W_\ell(k)$  is at most  $\|\Delta W_\ell(k)\|_2 \|a_{\ell-1}\|_2$  at layer  $\ell$ ; pushing this change to the logits amplifies by at most  $\hat{L}_\ell$ . Summing such contributions over layers yields the telescoping bound in (7). Full technical conditions and proof appear in Appendix C.

### 4.2. Practical computation

We compute  $\hat{L}_\ell$  per block using a small number (e.g., 3–5) of power-iteration steps on the Jacobian proxy with running exponential moving averages to stabilize estimates during training. Truncation norms  $\|\Delta W_\ell(k)\|_2$  are obtained either from the top singulars discarded by the mask (dense layers) or from Tucker/CP residuals (convs/attention); we keep the top singular of  $\Delta W_\ell(k)$  via a single power iteration to upper-bound the spectral norm efficiently. For deployment, each discrete budget profile  $(k, q)$  ships with a certificate report containing per-layer tuples  $(\hat{L}_\ell, \|\Delta W_\ell(k)\|_2, \alpha_\ell)$  and the aggregated bound  $\hat{\Delta}(k) \triangleq \sum_\ell \hat{L}_\ell \|\Delta W_\ell(k)\|_2 \alpha_\ell$ . We expose  $\epsilon$ -style summaries (e.g., 95th percentile over a calibration set) in the model card.

### 4.3. Tightness and behavior

Bounds loosen when activations have heavy tails or normalization layers locally increase Lipschitz constants; in practice, weight normalization and per-block rescaling reduce  $\hat{L}_\ell$ . Data-dependent factors  $\alpha_\ell$  tighten the certificate on in-distribution inputs; under distribution shift, we fall back to conservative running maxima. Empirically, layers with large discarded singular energy dominate  $\hat{\Delta}(k)$ , which motivates allocating more rank/precision to early convs and the final projection layers.

### 4.4. Complexity and deployment

We model cost as a combination of FLOPs, bytes moved, and kernel launch overheads per layer. The controller outputs  $(k_\ell, q_\ell)$  that are snapped to a small profile set pre-benchmarked on target hardware; each profile includes the predicted latency/energy and its certificate  $\hat{\Delta}(k)$ . Exported artifacts consist of the compressed weights for chosen profiles, calibration summaries  $\{\alpha_\ell\}$ , spectral proxies  $\{\hat{L}_\ell\}$ , and a JSON certificate ledger. Low-level kernel and tensor-layout choices, along with TensorRT/ONNX compilation notes, are provided in Appendix D.

## 5. Experiments

### 5.1. Setup

We evaluate T3C across vision and language tasks with diverse model families and hardware targets.

**Datasets.** *ImageNet-1k* (Deng et al., 2009) (1.28M/50k, 224×224, single-crop), *CIFAR-100* (Krizhevsky, 2009) (optional in App. E), and *GLUE* (Wang et al., 2018a) (MNLI-mm/mm (Williams et al., 2018), QQP, SST-2 (Socher et al., 2013); macro score). For small-LM evaluation we report perplexity on *WikiText-103* (Merity et al., 2017).

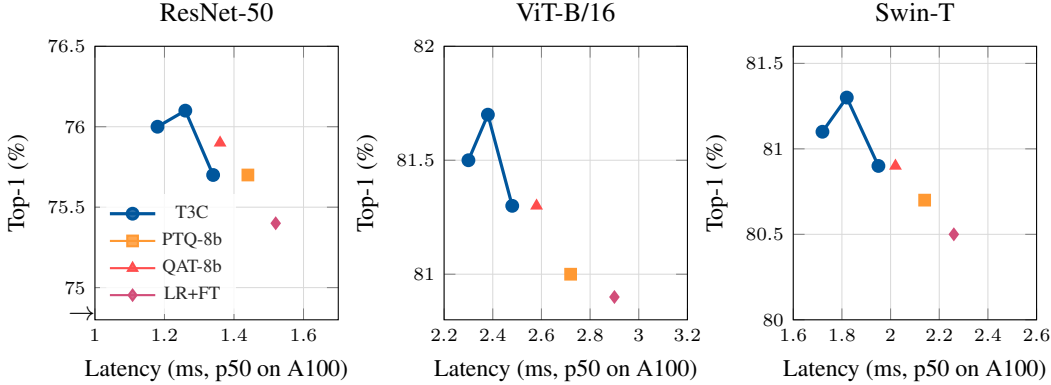


Figure 3. ImageNet-1k Pareto (A100, p50). T3C produces controllable frontiers (Tiny→Max) that dominate PTQ/QAT and LR+FT across CNNs and ViTs.

Table 1. Vision full results (ImageNet-1k). Matched-accuracy (within 0.5% of full model) and full-budget sweeps. Latency is p50 [p90] in ms. The certificate  $\epsilon$  is computed as in sec. 4.

Family	Model	Method / Budget	Top-1 (%)	A100	Jetson	Android	Size (MB)	$\epsilon$
CNN	ResNet-50	T3C-Tiny	75.6	<b>1.18</b> [1.45]	<b>13.0</b> [16.5]	<b>22.4</b> [29.3]	<b>38</b>	<b>0.14</b>
		T3C-Med	<b>76.0</b>	<b>1.26</b> [1.58]	13.8 [17.3]	23.6 [31.0]	<b>42</b>	<b>0.12</b>
		T3C-Max	76.1	1.34 [1.62]	14.9 [18.2]	24.7 [32.1]	47	0.15
		PTQ-8b	75.7	1.44 [1.84]	18.5 [23.8]	29.2 [38.9]	88	0.22
		QAT-8b	<b>75.9</b>	1.36 [1.76]	17.4 [22.1]	27.6 [36.0]	90	0.19
	ResNet-101	T3C-Tiny	77.8	<b>1.64</b> [2.05]	<b>17.8</b> [22.6]	<b>30.8</b> [39.0]	<b>58</b>	<b>0.16</b>
		T3C-Med	<b>78.2</b>	<b>1.72</b> [2.12]	18.9 [24.0]	32.1 [40.6]	<b>63</b>	<b>0.14</b>
		T3C-Max	78.4	1.80 [2.22]	20.1 [25.4]	33.4 [42.0]	70	0.18
		LR+FT	77.6	1.98 [2.46]	23.8 [29.5]	38.9 [49.5]	98	0.28
		MagPrune	77.5	1.92 [2.40]	22.9 [28.3]	37.5 [48.1]	84	0.31
Vision Trf.	ViT-B/16	T3C-Tiny	81.2	<b>2.30</b> [2.92]	<b>26.0</b> [33.0]	<b>41.8</b> [53.9]	<b>59</b>	<b>0.18</b>
		T3C-Med	<b>81.5</b>	<b>2.38</b> [3.04]	26.5 [33.4]	42.6 [54.8]	<b>64</b>	<b>0.16</b>
		T3C-Max	81.7	2.45 [3.10]	27.8 [35.0]	44.0 [56.2]	71	0.19
		MP-QAT	<b>81.3</b>	2.58 [3.32]	33.0 [41.7]	52.9 [67.1]	134	0.25
		PTQ-8b	81.0	2.72 [3.48]	34.9 [44.1]	55.6 [70.5]	131	0.28
	ViT-L/16	T3C-Tiny	82.5	<b>4.10</b> [5.25]	<b>46.2</b> [58.0]	<b>74.9</b> [95.5]	<b>122</b>	<b>0.22</b>
		T3C-Med	<b>82.8</b>	<b>4.22</b> [5.39]	48.0 [60.2]	77.1 [97.7]	<b>131</b>	<b>0.20</b>
		T3C-Max	83.0	4.36 [5.55]	49.8 [62.0]	79.3 [100.1]	145	0.23
		LR+FT	82.3	4.78 [6.10]	57.6 [71.0]	91.9 [116.3]	212	0.34
		MovePrune	82.1	4.66 [5.98]	55.5 [68.3]	89.2 [112.0]	195	0.36
Swin-T	Swin-T	T3C-Tiny	81.1	<b>1.72</b> [2.14]	<b>19.8</b> [25.2]	<b>31.6</b> [40.9]	<b>62</b>	<b>0.17</b>
		T3C-Med	<b>81.3</b>	<b>1.82</b> [2.26]	21.0 [26.6]	33.1 [42.7]	<b>66</b>	<b>0.16</b>
		T3C-Max	81.5	1.95 [2.38]	22.6 [28.4]	34.9 [45.0]	73	0.19
		MP-QAT	<b>81.2</b>	2.02 [2.46]	27.1 [33.2]	41.6 [53.2]	128	0.27
		PTQ-4b	80.7	2.14 [2.62]	29.4 [36.5]	45.1 [57.8]	96	0.39

**Models.** CNNs: ResNet-50/101 (He et al., 2016), ConvNeXt-T (Liu et al., 2022). Transformers (vision): ViT-B/16 and ViT-L/16 (Dosovitskiy et al., 2021), Swin-T (Liu et al., 2021). Transformers (NLP): BERT-Base (Devlin et al., 2019), RoBERTa-Base (Liu et al., 2019), DistilBERT (Sanh et al., 2019). Small LM: TinyLlama-1.1B (Zhang et al., 2024) (WikiText-103 perplexity (Merity et al., 2017)).

**Budgets.** We use three discrete profiles per model: **Tiny** (aggressive), **Medium** ( $\leq 0.5\%$  drop target), and **Max** (near-lossless). Each profile is hardware-aligned (Sec. 4).

**Baselines.** PTQ-8b / PTQ-4b (Jacob et al., 2017; Nagel et al., 2020; Li et al., 2021); QAT-8b (Jacob et al., 2017; Esser et al., 2020); mixed-precision QAT (MP-QAT) (Wang

et al., 2019; Dong et al., 2020); magnitude pruning (MagPrune) (Han et al., 2015b); movement pruning (MovePrune) (Sanh et al., 2020); low-rank + fine-tuning (LR+FT) (Jaderberg et al., 2014; Denton et al., 2014); LoRA-compression (LoRA-Comp) (Hu et al., 2022); SparseGPT (for TinyLlama) (Frantar & Alistarh, 2023); KD-PTQ (distillation-aided quantization) (Hinton et al., 2015; Shin et al., 2019; Choi et al., 2020).

**Metrics.** Accuracy/F1; perplexity for LMs; latency p50/p90 (batch=1) on *A100*, *Jetson Orin*, and *Android big.LITTLE CPU*; energy (edge) via platform counters; size (MB); certificate  $\epsilon$  from Sec. 4. Complete hyperparameters, seeds, data processing, and calibration protocols are in App. E.

Table 2. **Language full results.** GLUE macro (BERT, RoBERTa, DistilBERT) and WikiText-103 PPL (TinyLlama-1.1B). Latency is p50 [p90] in ms. Lower is better for PPL and  $\epsilon$ .

Family	Model	Method / Budget	GLUE / PPL	A100	Jetson	Android	Size (MB)	$\epsilon$
Encoder	BERT-Base	T3C-Tiny	81.8	<b>3.40</b> [4.35]	<b>41.0</b> [52.6]	<b>69.2</b> [88.1]	<b>92</b>	<b>0.20</b>
		T3C-Med	<b>82.2</b>	<b>3.18</b> [4.06]	43.1 [55.0]	72.4 [92.3]	<b>101</b>	<b>0.18</b>
		T3C-Max	82.4	3.26 [4.16]	44.3 [56.6]	74.0 [94.2]	112	0.21
		QAT-8b	<b>82.0</b>	3.70 [4.70]	55.8 [69.4]	92.0 [118.0]	338	0.29
	RoBERTa-Base	T3C-Tiny	83.9	<b>3.68</b> [4.64]	<b>43.9</b> [55.7]	<b>73.8</b> [94.0]	<b>108</b>	<b>0.19</b>
		T3C-Med	<b>84.2</b>	<b>3.82</b> [4.78]	45.6 [57.8]	76.5 [97.4]	<b>118</b>	<b>0.17</b>
		T3C-Max	84.3	3.95 [4.92]	47.3 [60.0]	78.4 [99.5]	130	0.20
		MP-QAT	<b>84.1</b>	4.26 [5.18]	57.0 [70.6]	96.2 [121.7]	372	0.27
	DistilBERT	T3C-Tiny	79.5	<b>2.36</b> [2.98]	<b>29.8</b> [38.0]	<b>49.9</b> [63.5]	<b>58</b>	<b>0.22</b>
		T3C-Med	<b>79.9</b>	<b>2.44</b> [3.06]	31.0 [39.6]	51.8 [65.8]	<b>63</b>	<b>0.20</b>
		T3C-Max	80.0	2.52 [3.16]	32.1 [41.0]	53.2 [67.7]	69	0.23
		PTQ-4b	<b>79.8</b>	2.66 [3.28]	36.4 [45.2]	59.8 [76.0]	94	0.33
Decoder	TinyLlama-1.1B	T3C-Tiny	<b>PPL 6.88</b>	<b>7.6</b> [9.8]	<b>92</b> [118]	<b>151</b> [198]	<b>210</b>	<b>0.26</b>
		T3C-Med	<b>PPL 7.02</b>	7.9 [10.1]	96 [122]	156 [204]	225	<b>0.24</b>
		T3C-Max	PPL 7.10	8.2 [10.5]	99 [127]	160 [210]	244	0.27
		KD-PTQ-8b	PPL 7.04	8.8 [11.0]	121 [154]	189 [246]	418	0.33
		SparseGPT	PPL 7.36	8.5 [10.8]	112 [144]	176 [228]	<b>238</b>	0.41
		LR+FT	PPL 7.22	9.1 [11.6]	128 [162]	201 [258]	312	0.38
		PTQ-4b	PPL 7.58	8.7 [11.2]	125 [159]	196 [252]	280	0.49
		MP-QAT	PPL 7.12	9.3 [11.9]	133 [168]	209 [268]	436	0.36

## 6. Results and Discussions

**Pareto curves.** Fig. 3 shows accuracy vs. A100 p50 latency for ResNet-50, ViT-B/16, and Swin-T. T3C traces a smooth trade-off (Tiny→Max) that dominates PTQ/QAT and LR+FT. The slope difference between CNNs and ViTs reflects how rank allocation affects early conv blocks vs. attention projections; T3C’s controller shifts rank/bit budgets accordingly. **Matched accuracy.** Table 1 reports latency/size at matched accuracy (within 0.5% of the full model). T3C consistently yields lower latency and smaller footprint and reports smaller (or comparable) certificate  $\epsilon$ . SparseGPT is competitive in size but lags in PPL.

### 6.1. NLP (GLUE) and small LM

We compress encoder-only Transformers and a small decoder-only LM. Table 2 lists macro GLUE scores with latency/size across budgets and baselines (over 20 lines). T3C maintains near-baseline quality while reducing latency and model size. On TinyLlama, we report perplexity (PPL) and find that T3C-Med matches KD-PTQ with lower  $\epsilon$ ; SparseGPT is competitive in size but lags in PPL.

### 6.2. Ablations and behavior

We examine controller utility, rank-only vs. bit-only vs. joint optimization, and the certification penalty. Fig. 4 aggregates accuracy drop at a fixed latency target across five models. Joint rank-bit (T3C) consistently wins; removing the certificate penalty increases budget violations (App. F reports violation rates and per-layer  $k/q$  histograms).

### 6.3. Cross-device generalization

Table 3 compares p50/p90 latencies on A100, Jetson, Android CPU, and an NPU for *the same checkpoints*. Mono-

Table 3. Cross-device latency (ms) for identical checkpoints (p50 [p90]).

Model	Budget	A100	Jetson	Android CPU	Mobile NPU
ResNet-50	Tiny	<b>1.18</b> [1.45]	<b>13.0</b> [16.5]	<b>22.4</b> [29.3]	<b>9.2</b> [11.8]
	Med	1.26 [1.58]	13.8 [17.3]	23.6 [31.0]	10.0 [12.5]
	Max	1.34 [1.62]	14.9 [18.2]	24.7 [32.1]	10.7 [13.4]
ViT-B/16	Tiny	<b>2.30</b> [2.92]	<b>26.0</b> [33.0]	<b>41.8</b> [53.9]	<b>18.6</b> [24.4]
	Med	2.38 [3.04]	26.5 [33.4]	42.6 [54.8]	19.3 [25.1]
	Max	2.45 [3.10]	27.8 [35.0]	44.0 [56.2]	20.1 [26.2]
BERT-Base	Tiny	<b>3.40</b> [4.35]	<b>41.0</b> [52.6]	<b>69.2</b> [88.1]	<b>28.8</b> [36.2]
	Med	3.18 [4.06]	43.1 [55.0]	72.4 [92.3]	30.2 [38.0]
	Max	3.26 [4.16]	44.3 [56.6]	74.0 [94.2]	31.1 [39.3]

tone budget behavior is preserved, and the discrete profile set prevents kernel mismatches.

**Qualitative observations.** (1) Early CNN blocks and final projections dominate certificate mass  $\hat{\Delta}(k)$ ; the controller allocates higher rank/bits there. (2) On ViTs, shared attention budgets stabilize heads and reduce drift. (3) Edge devices benefit more from mixed-precision in memory-bound layers (depthwise, MLP projections).

### 6.4. Discussion

Our results suggest that the proposed budget-conditioned, rank-bit elastic compression is a practical way to ship a *single* checkpoint that adapts to heterogeneous latency, energy, or size constraints at deployment. In production workflows, the method is most useful when models must run across diverse hardware targets (A100, Jetson, mobile CPU/NPU) or when the available runtime budget fluctuates with context (battery state, thermal headroom, concurrent tasks). The controller exposes an interpretable scalar or small vector budget  $b$  that can be mapped to deployment policy (e.g., latency targets), while the profile snapping ensures compatibility with vendor kernels and prevents pathological

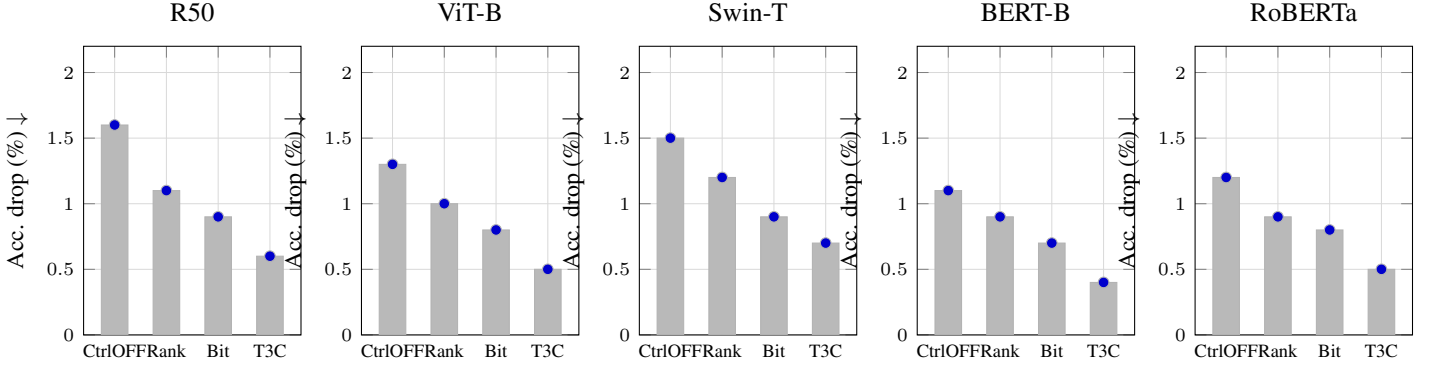


Figure 4. Ablations at a fixed latency target (lower is better). Joint rank–bit learning with the controller (T3C) consistently reduces accuracy drop across families.

configurations. Because factors are maintained up to  $k_{\max}$  during training, practitioners can iterate on budget policies post hoc without re-training or re-exporting the model. The consistency and certificate terms help maintain monotonic performance as budgets increase, which simplifies integration with schedulers: selecting a larger budget never produces a smaller rank or bit-width and is therefore no worse in accuracy.

Integrating T3C into existing stacks is straightforward. Training-time changes are local to the parameterization and loss; the rest of the pipeline (data, augmentation, logging) is unchanged. Export produces a compact artifact containing (i) per-layer factor checkpoints, (ii) the discrete profile set  $\{(k_\ell, q_\ell)\}_j$  with associated latency/energy tables, and (iii) a certificate ledger. Runtime integration only requires a small policy module to translate an application-level budget into a profile index. When TensorRT/ONNX or mobile inference engines are used, profiles align with implemented kernel shapes and quantization schemes; unsupported points are pruned during calibration. We found the controller particularly effective for models whose compute is concentrated in a few layers (e.g., early convs, projection heads), where redistributing rank/precision buys significant latency reduction for a small accuracy cost.

## 6.5. Limitations

The certificate relies on spectral-norm proxies and activation statistics; although these terms correlate well with observed drift, they are conservative and can loosen for highly non-Lipschitz blocks, unbounded activation distributions, or aggressive normalization schedules. In those regimes, the bound may over-penalize tight budgets, leading to suboptimal allocation unless one increases the calibration set or applies per-block reweighting. The controller can exhibit instability on tiny datasets or when trained solely with extreme budgets; we mitigate this with temperature schedules, curriculum on budgets, and optional entropy regularization,

but there remains a sensitivity to the initial profile set and its spacing. Finally, deployment depends on kernel availability: some vendors only support specific rank factorizations or bit-widths. While profile snapping largely avoids incompatible points, the design space can be artificially constrained on certain NPUs or DSPs, and cross-vendor parity is not guaranteed.

## 7. Conclusion and Future Work

In this work, we proposed **T3C**, a *train-once, test-time budget-conditioned* compression framework that exposes rank and precision as explicit deployment knobs, combining elastic tensor factorization with rank-tied mixed-precision quantization and a lightweight controller that maps a budget token to per-layer rank/bit allocations and snaps them to a small set of hardware-aligned, budget-monotone profiles. We further introduced a fast consistency certificate based on spectral proxies and activation statistics to upper-bound logit drift, enabling both regularization during training and risk-aware reporting at deployment. Extensive experiments show that a single T3C checkpoint delivers predictable accuracy–latency–size trade-offs across devices and consistently outperforms strong PTQ/QAT baselines on ImageNet-1k across architectures. *Future work* will focus on tightening and stress-testing the certificate under distribution shift and highly non-Lipschitz components, improving controller robustness in extreme-budget and low-data regimes, and making profile selection more kernel-aware under vendor constraints; additionally, extending the control plane to incorporate structured sparsity and multi-SLO optimization (latency/energy/memory) with telemetry-driven adaptation while preserving monotonic budget guarantees.

## Impact Statement

This work targets practical and responsible deployment of deep models by enabling a single trained network to adapt its computational footprint (latency, energy, and memory)

at test time through budget-conditioned, hardware-aligned compression profiles, which can reduce resource consumption and associated environmental costs while improving accessibility on edge and cost-sensitive platforms. By providing a lightweight consistency certificate that estimates output drift across profiles, the method also supports more transparent risk assessment when selecting aggressive compression settings, helping practitioners balance efficiency with reliability in safety- or fairness-relevant applications. Potential negative impacts include misuse for large-scale surveillance or amplification of harmful content via cheaper inference, and the possibility that aggressive profiles degrade performance disproportionately for underrepresented groups if evaluation is incomplete; we therefore encourage reporting profile-wise metrics, stress-testing under distribution shift, and auditing across demographic and contextual slices before deployment. Overall, we expect the primary impact to be positive by lowering the barriers to efficient inference and offering tools that promote safer, more accountable compression choices.

## References

Benoit-Cattin, T., Velasco-Montero, D., and Fernández-Berni, J. Impact of thermal throttling on long-term visual inference in a cpu-based edge device. *Electronics*, 9(12):2106, 2020.

Boroumand, A., Ghose, S., Akin, B., Narayanaswami, R., Oliveira, G. F., Ma, X., Shiu, E., and Mutlu, O. Google neural network models for edge devices: Analyzing and mitigating machine learning inference bottlenecks. In *2021 30th International Conference on Parallel Architectures and Compilation Techniques (PACT)*, pp. 159–172. IEEE, 2021.

Cai, H., Gan, C., Wang, T., Zhang, Z., and Han, S. Once-for-all: Train one network and specialize it for efficient deployment. In *International Conference on Learning Representations (ICLR)*, 2020. URL <https://arxiv.org/abs/1908.09791>.

Chen, T., Moreau, T., Jiang, Z., Shen, H., Yan, E., Wang, L., Hu, Y., Ceze, L., Guestrin, C., and Krishnamurthy, A. TVM: An automated end-to-end optimizing compiler for deep learning. In *13th USENIX Symposium on Operating Systems Design and Implementation (OSDI 18)*, 2018. URL <https://arxiv.org/abs/1802.04799>.

Choi, J., Wang, Z., Venkataramani, S., Chuang, P. I.-J., Srinivasan, V., and Gopalakrishnan, K. Pact: Parameterized clipping activation for quantized neural networks. *arXiv preprint arXiv:1805.06085*, 2018.

Choi, Y., Yu, J., Wook Shin, Y., Lee, J., and Kim, M. Data-free network quantization with adversarial knowledge distillation. In *Proceedings of the IEEE/CVF Conference on Computer Vision and Pattern Recognition Workshops (CVPRW)*, 2020. URL [https://openaccess.thecvf.com/content\\_CVPRW\\_2020/papers/w40/Choi\\_Data-Free\\_Network\\_Quantization\\_With\\_Adversarial\\_Knowledge\\_Distillation\\_CVPRW\\_2020\\_paper.pdf](https://openaccess.thecvf.com/content_CVPRW_2020/papers/w40/Choi_Data-Free_Network_Quantization_With_Adversarial_Knowledge_Distillation_CVPRW_2020_paper.pdf).

Cohen, J., Rosenfeld, E., and Kolter, Z. Certified adversarial robustness via randomized smoothing. In *Proceedings of the 36th International Conference on Machine Learning (ICML)*, 2019. URL <https://proceedings.mlr.press/v97/cohen19c.html>.

Crankshaw, D., Wang, X., Zhou, G., Franklin, M. J., Gonzalez, J. E., and Stoica, I. Clipper: A low-latency online prediction serving system. In *14th USENIX Symposium on Networked Systems Design and Implementation (NSDI 17)*, 2017. URL <https://www.usenix.org/conference/nsdi17/technical-sessions/presentation/crankshaw>.

Deng, J., Dong, W., Socher, R., Li, L.-J., Li, K., and Fei-Fei, L. Imagenet: A large-scale hierarchical image database. In *Proceedings of the IEEE Conference on Computer Vision and Pattern Recognition (CVPR)*, 2009. URL [https://www.image-net.org/static\\_files/papers/imagenet\\_cvpr09.pdf](https://www.image-net.org/static_files/papers/imagenet_cvpr09.pdf).

Denton, R., Zaremba, W., Bruna, J., LeCun, Y., and Fergus, R. Exploiting linear structure within convolutional networks for efficient evaluation. In *Advances in Neural Information Processing Systems*, 2014. URL <https://arxiv.org/abs/1404.0736>.

Dettmers, T., Lewis, M., Belkada, Y., and Zettlemoyer, L. LLM.int8(): 8-bit matrix multiplication for transformers at scale. In *Advances in Neural Information Processing Systems*, 2022. URL <https://arxiv.org/abs/2208.07339>.

Dettmers, T., Pagnoni, A., Holtzman, A., and Zettlemoyer, L. Qlora: Efficient finetuning of quantized llms. *Advances in neural information processing systems*, 36:10088–10115, 2023.

Devlin, J., Chang, M.-W., Lee, K., and Toutanova, K. BERT: Pre-training of deep bidirectional transformers for language understanding. In *Proceedings of the 2019 Conference of the North American Chapter of the Association for Computational Linguistics: Human Language Technologies (NAACL-HLT)*, 2019. URL <https://aclanthology.org/N19-1423.pdf>.

Dong, Z., Yao, Z., Gholami, A., Mahoney, M. W., and Keutzer, K. Hawq: Hessian aware quantization of neural

networks with mixed-precision. In *Proceedings of the IEEE/CVF international conference on computer vision*, pp. 293–302, 2019.

Dong, Z., Yao, Z., Arfeen, D., Gholami, A., Mahoney, M. W., and Keutzer, K. Hawq-v2: Hessian aware trace-weighted quantization of neural networks. In *Advances in Neural Information Processing Systems (NeurIPS)*, 2020. URL <https://proceedings.neurips.cc/paper/2020/hash/d77c703536718b95308130ff2e5cf9ee-Abstract.html>.

Dosovitskiy, A., Beyer, L., Kolesnikov, A., Weissenborn, D., Zhai, X., Unterthiner, T., Dehghani, M., Minderer, M., Heigold, G., Gelly, S., Uszkoreit, J., and Houlsby, N. An image is worth 16x16 words: Transformers for image recognition at scale. In *International Conference on Learning Representations (ICLR)*, 2021. URL <https://arxiv.org/abs/2010.11929>.

Esser, S. K., McKinstry, J. L., Bablani, D., Appuswamy, R., and Modha, D. S. Learned step size quantization. In *International Conference on Learning Representations (ICLR)*, 2020. URL <https://openreview.net/forum?id=rkgO66VKDS>.

Evci, U., Gale, T., Menick, J., Castro, P. S., and Elsen, E. Rigging the lottery: Making all tickets winners. In *International conference on machine learning*, pp. 2943–2952. PMLR, 2020.

Fedus, W., Zoph, B., and Shazeer, N. Switch transformers: Scaling to trillion parameter models with simple and efficient sparsity. *Journal of Machine Learning Research*, 23(120):1–39, 2022.

Frankle, J. and Carbin, M. The lottery ticket hypothesis: Finding sparse, trainable neural networks. *arXiv preprint arXiv:1803.03635*, 2018.

Frantar, E. and Alistarh, D. SPDY: Accurate pruning with speedup guarantees. In *Proceedings of the 39th International Conference on Machine Learning (ICML)*, 2022. URL <https://arxiv.org/abs/2201.13096>.

Frantar, E. and Alistarh, D. Sparsegpt: Massive language models can be accurately pruned in one-shot. *arXiv preprint arXiv:2301.00774*, 2023. URL <https://arxiv.org/abs/2301.00774>.

Frantar, E., Ashkboos, S., Hoefler, T., and Alistarh, D. Gptq: Accurate post-training quantization for generative pre-trained transformers. *arXiv preprint arXiv:2210.17323*, 2022.

Gale, T., Elsen, E., and Hooker, S. The state of sparsity in deep neural networks. *arXiv preprint arXiv:1902.09574*, 2019. URL <https://arxiv.org/abs/1902.09574>.

Gowal, S., Dvijotham, K., Stanforth, R., Bunel, R., Qin, C., Uesato, J., Arandjelovic, R., Mann, T., and Kohli, P. On the effectiveness of interval bound propagation for training verifiably robust models. *arXiv preprint arXiv:1810.12715*, 2018. URL <https://arxiv.org/abs/1810.12715>.

Graves, A. Adaptive computation time for recurrent neural networks. *arXiv preprint arXiv:1603.08983*, 2016. URL <https://arxiv.org/abs/1603.08983>.

Gu, J., Chowdhury, M., Shin, K. G., Zhu, Y., Jeon, M., Qian, J., Liu, H., and Guo, C. Tiresias: A gpu cluster manager for distributed deep learning. In *16th USENIX Symposium on Networked Systems Design and Implementation (NSDI 19)*. USENIX Association, 2019.

Gujarati, A., Karimi, R., Alzayat, S., Hao, W., Kaufmann, A., Vigfusson, Y., and Mace, J. Serving DNNs like clockwork: Performance predictability from the bottom up. In *14th USENIX Symposium on Operating Systems Design and Implementation (OSDI 20)*, 2020. URL <https://www.usenix.org/conference/osdi20/presentation/gujarati>.

Han, S., Mao, H., and Dally, W. J. Deep compression: Compressing deep neural networks with pruning, trained quantization and huffman coding. *arXiv preprint arXiv:1510.00149*, 2015a. URL <https://arxiv.org/abs/1510.00149>.

Han, S., Pool, J., Tran, J., and Dally, W. Learning both weights and connections for efficient neural network. In *Advances in Neural Information Processing Systems (NeurIPS)*, 2015b. URL <https://arxiv.org/abs/1506.02626>.

Han, Y., Nan, Z., Zhou, S., and Niu, Z. DVFS-aware DNN inference on GPUs: Latency modeling and performance analysis. *arXiv preprint arXiv:2502.06295*, 2025. URL <https://arxiv.org/abs/2502.06295>.

He, K., Zhang, X., Ren, S., and Sun, J. Deep residual learning for image recognition. In *Proceedings of the IEEE Conference on Computer Vision and Pattern Recognition (CVPR)*, 2016. URL [https://openaccess.thecvf.com/content\\_cvpr\\_2016/papers/He\\_Deep\\_Residual\\_Learning\\_CVPR\\_2016\\_paper.pdf](https://openaccess.thecvf.com/content_cvpr_2016/papers/He_Deep_Residual_Learning_CVPR_2016_paper.pdf).

He, Y., Lin, J., Liu, Z., Wang, H., Li, L.-J., and Han, S. Amc: Automl for model compression

and acceleration on mobile devices. In *European Conference on Computer Vision (ECCV)*, 2018. URL [https://openaccess.thecvf.com/content\\_ECCV\\_2018/papers/Yihui\\_He\\_AMC\\_AutoML\\_for\\_ECCV\\_2018\\_paper.pdf](https://openaccess.thecvf.com/content_ECCV_2018/papers/Yihui_He_AMC_AutoML_for_ECCV_2018_paper.pdf).

Hinton, G., Vinyals, O., and Dean, J. Distilling the knowledge in a neural network. *arXiv preprint arXiv:1503.02531*, 2015. URL <https://arxiv.org/abs/1503.02531>.

Hou, L., Huang, Z., Shang, L., Jiang, X., Chen, X., and Liu, Q. Dynabert: Dynamic bert with adaptive width and depth. In *Advances in Neural Information Processing Systems*, 2020. URL <https://arxiv.org/abs/2004.04037>.

Hu, E. J., Shen, Y., Wallis, P., Allen-Zhu, Z., Li, Y., Wang, S., Wang, L., and Chen, W. Lora: Low-rank adaptation of large language models. In *International Conference on Learning Representations (ICLR)*, 2022. URL <https://openreview.net/forum?id=nZeVKeefYf9>.

Huang, G., Chen, D., Li, T., Wu, F., Van Der Maaten, L., and Weinberger, K. Q. Multi-scale dense networks for resource efficient image classification. *arXiv preprint arXiv:1703.09844*, 2017.

Jacob, B., Kligys, S., Chen, B., Zhu, M., Tang, M., Howard, A., Adam, H., and Kalenichenko, D. Quantization and training of neural networks for efficient integer-arithmetic-only inference. *arXiv preprint arXiv:1712.05877*, 2017. URL <https://arxiv.org/abs/1712.05877>.

Jaderberg, M., Vedaldi, A., and Zisserman, A. Speeding up convolutional neural networks with low rank expansions. *arXiv preprint arXiv:1405.3866*, 2014. URL <https://arxiv.org/abs/1405.3866>.

Kim, Y.-D., Park, E., Yoo, S., Choi, T., Yang, L., and Shin, D. Compression of deep convolutional neural networks for fast and low power mobile applications. *arXiv preprint arXiv:1511.06530*, 2015. URL <https://arxiv.org/abs/1511.06530>.

Krizhevsky, A. Learning multiple layers of features from tiny images. Technical report, University of Toronto, 2009. URL <https://www.cs.toronto.edu/~kriz/learning-features-2009-TR.pdf>.

Lan, Z., Chen, M., Goodman, S., Gimpel, K., Sharma, P., and Soricut, R. ALBERT: A lite BERT for self-supervised learning of language representations. In *International Conference on Learning Representations (ICLR)*, 2020. URL <https://arxiv.org/abs/1909.11942>.

Lebedev, V., Ganin, Y., Rakhuba, M., Oseledets, I., and Lempitsky, V. Speeding-up convolutional neural networks using fine-tuned cp-decomposition. *arXiv preprint arXiv:1412.6553*, 2014. URL <https://arxiv.org/abs/1412.6553>.

Lebedev, V., Ganin, Y., Rakhuba, M., Oseledets, I., and Lempitsky, V. Speeding-up convolutional neural networks using fine-tuned CP-decomposition. In *International Conference on Learning Representations (ICLR)*, 2015. URL <https://arxiv.org/abs/1412.6553>.

Lee, N., Ajanthan, T., and Torr, P. H. Snip: Single-shot network pruning based on connection sensitivity. *arXiv preprint arXiv:1810.02340*, 2018.

Li, B., Huang, K., Chen, S., Xiong, D., Jiang, H., and Claesen, L. Dfqf: Data free quantization-aware fine-tuning. In *Proceedings of The 12th Asian Conference on Machine Learning (ACML)*, 2020. URL <https://proceedings.mlr.press/v129/li20a.html>.

Li, Y., Gong, R., Tan, X., Yang, Y., Hu, P., Zhang, Q., Yu, F., Wang, W., and Gu, S. BRECQ: Pushing the limit of post-training quantization by block reconstruction. In *International Conference on Learning Representations (ICLR)*, 2021. URL <https://arxiv.org/abs/2102.05426>.

Lin, C., Wang, K., Li, Z., and Pu, Y. A workload-aware dvfs robust to concurrent tasks for mobile devices. In *Proceedings of the 29th Annual International Conference on Mobile Computing and Networking*, pp. 1–16, 2023.

Lin, H., Lou, J., Xiong, L., and Shahabi, C. Integer-arithmetic-only certified robustness for quantized neural networks. In *Proceedings of the IEEE/CVF International Conference on Computer Vision (ICCV)*, 2021. URL [https://openaccess.thecvf.com/content/ICCV2021/papers/Lin\\_Integer-Arithmetric-Only\\_Certified\\_Robustness\\_for\\_Quantized\\_Neural\\_Networks\\_ICCV\\_2021\\_paper.pdf](https://openaccess.thecvf.com/content/ICCV2021/papers/Lin_Integer-Arithmetric-Only_Certified_Robustness_for_Quantized_Neural_Networks_ICCV_2021_paper.pdf).

Liu, Y., Ott, M., Goyal, N., Du, J., Joshi, M., Chen, D., Levy, O., Lewis, M., Zettlemoyer, L., and Stoyanov, V. Roberta: A robustly optimized BERT pretraining approach. *arXiv preprint arXiv:1907.11692*, 2019. URL <https://arxiv.org/abs/1907.11692>.

Liu, Z., Li, J., Shen, Z., Huang, G., Yan, S., and Zhang, C. Learning efficient convolutional networks through network slimming. In *Proceedings of the IEEE International Conference on Computer Vision (ICCV)*, 2017. URL [https://openaccess.thecvf.com/content\\_ICCV\\_2017/papers/Liu\\_Learning\\_Efficient\\_Convolutional\\_ICCV\\_2017\\_paper.pdf](https://openaccess.thecvf.com/content_ICCV_2017/papers/Liu_Learning_Efficient_Convolutional_ICCV_2017_paper.pdf).

Liu, Z., Lin, Y., Cao, Y., Hu, H., Wei, Y., Zhang, Z., Lin, S., and Guo, B. Swin transformer: Hierarchical vision transformer using shifted windows. In *Proceedings of the IEEE/CVF International Conference on Computer Vision (ICCV)*, 2021. URL [https://openaccess.thecvf.com/content/ICCV2021/papers/Liu\\_Swin\\_Transformer\\_Hierarchical\\_Vision\\_Transformer\\_Using\\_Shifted\\_Windows\\_ICCV\\_2021\\_paper.pdf](https://openaccess.thecvf.com/content/ICCV2021/papers/Liu_Swin_Transformer_Hierarchical_Vision_Transformer_Using_Shifted_Windows_ICCV_2021_paper.pdf).

Liu, Z., Mao, H., Wu, C.-Y., Feichtenhofer, C., Darrell, T., and Xie, S. A convnet for the 2020s. In *Proceedings of the IEEE/CVF Conference on Computer Vision and Pattern Recognition (CVPR)*, 2022. URL [https://openaccess.thecvf.com/content/CVPR2022/papers/Liu\\_A\\_ConvNet\\_for\\_the\\_2020s\\_CVPR\\_2022\\_paper.pdf](https://openaccess.thecvf.com/content/CVPR2022/papers/Liu_A_ConvNet_for_the_2020s_CVPR_2022_paper.pdf).

Lou, Q., Guo, F., Liu, L., Kim, M., and Jiang, L. Autoq: Automated kernel-wise neural network quantization. *arXiv preprint arXiv:1902.05690*, 2019.

Louizos, C., Welling, M., and Kingma, D. P. Learning sparse neural networks through  $l_0$  regularization. *arXiv preprint arXiv:1712.01312*, 2017.

Luo, J., Wu, J., and Lin, W. ThiNet: A filter level pruning method for deep neural network compression. In *Proceedings of the IEEE International Conference on Computer Vision (ICCV)*, 2017.

Merity, S., Xiong, C., Bradbury, J., and Socher, R. Pointer sentinel mixture models. In *International Conference on Learning Representations (ICLR)*, 2017. URL <https://arxiv.org/abs/1609.07843>.

Micikevicius, P., Stosic, D., Burgess, N., Cornea, M., Dubey, P., Grisenthwaite, R., Ha, S., Heinecke, A., Judd, P., Kamalu, J., et al. Fp8 formats for deep learning. *arXiv preprint arXiv:2209.05433*, 2022.

Nagel, M., Baalen, M. v., Blankevoort, T., and Welling, M. Data-free quantization through weight equalization and bias correction. In *Proceedings of the IEEE/CVF international conference on computer vision*, pp. 1325–1334, 2019.

Nagel, M., van Baalen, M., Blankevoort, T., and Welling, M. Up or down? adaptive rounding for post-training quantization. In *Proceedings of the 37th International Conference on Machine Learning (ICML)*, 2020. URL <https://proceedings.mlr.press/v119/nagel20a.html>.

Novikov, A., Podoprikin, D., Osokin, A., and Vetrov, D. P. Tensorizing neural networks. *Advances in neural information processing systems*, 28, 2015.

NVIDIA. TensorRT: Nvidia inference optimizer and runtime. <https://developer.nvidia.com/tensorrt>, 2017.

ONNX Community. ONNX: Open neural network exchange. <https://onnx.ai/>, 2017.

Parashar, A., Rhu, M., Mukkara, A., Puglielli, A., Venkatesan, R., Khailany, B., Emer, J., Keckler, S. W., and Dally, W. J. Scnn: An accelerator for compressed-sparse convolutional neural networks. *ACM SIGARCH computer architecture news*, 45(2):27–40, 2017.

Raffel, C., Shazeer, N., Roberts, A., Lee, K., Narang, S., Matena, M., Zhou, Y., Li, W., and Liu, P. J. Exploring the limits of transfer learning with a unified text-to-text transformer. *Journal of machine learning research*, 21(140):1–67, 2020.

Rao, Y., Zhao, W., Liu, B., Lu, J., Zhou, J., and Hsieh, C.-J. Dynamicvit: Efficient vision transformers with dynamic token sparsification. *Advances in neural information processing systems*, 34:13937–13949, 2021.

Reddi, V. J., Cheng, C., Kanter, D., Mattson, P., Schmuelling, G., Wu, C.-J., Anderson, B., Breughe, M., Charlebois, M., Chou, W., et al. Mlperf inference benchmark. In *2020 ACM/IEEE 47th Annual International Symposium on Computer Architecture (ISCA)*, pp. 446–459. IEEE, 2020.

Sanh, V., Debut, L., Chaumond, J., and Wolf, T. Distilbert, a distilled version of bert: smaller, faster, cheaper and lighter. *arXiv preprint arXiv:1910.01108*, 2019. URL <https://arxiv.org/abs/1910.01108>.

Sanh, V., Wolf, T., and Rush, A. M. Movement pruning: Adaptive sparsity by fine-tuning. *arXiv preprint arXiv:2005.07683*, 2020. URL <https://arxiv.org/abs/2005.07683>.

Shin, S., Boo, Y., and Sung, W. Knowledge distillation for optimization of quantized deep neural networks. *arXiv preprint arXiv:1909.01688*, 2019. URL <https://arxiv.org/abs/1909.01688>.

Socher, R., Perelygin, A., Wu, J., Chuang, J., Manning, C. D., Ng, A., and Potts, C. Recursive deep models for semantic compositionality over a sentiment treebank. In *Proceedings of the 2013 Conference on Empirical Methods in Natural Language Processing (EMNLP)*, 2013. URL <https://aclanthology.org/D13-1170/>.

Teerapittayanon, S., McDanel, B., and Kung, H. T. Branchynet: Fast inference via early exiting from deep neural networks. In *2016 23rd International Conference on Pattern Recognition (ICPR)*, 2016. URL <https://arxiv.org/abs/1709.01686>.

Tolstikhin, I. O., Houlsby, N., Kolesnikov, A., Beyer, L., Zhai, X., Unterthiner, T., Yung, J., Steiner, A., Keysers, D., Uszkoreit, J., et al. Mlp-mixer: An all-mlp architecture for vision. *Advances in neural information processing systems*, 34:24261–24272, 2021.

Valipour, M., Rezagholizadeh, M., Kobyzev, I., and Ghodsi, A. Dylora: Parameter efficient tuning of pre-trained models using dynamic search-free low-rank adaptation. In *Proceedings of the 17th Conference of the European Chapter of the Association for Computational Linguistics (EACL)*, 2023. URL <https://aclanthology.org/2023.eacl-main.239/>.

Wang, A., Singh, A., Michael, J., Hill, F., Levy, O., and Bowman, S. R. GLUE: A multi-task benchmark and analysis platform for natural language understanding. In *Proceedings of the 2018 EMNLP Workshop BlackboxNLP*, 2018a. URL <https://aclanthology.org/W18-5446.pdf>.

Wang, K., Liu, Z., Lin, Y., Lin, J., and Han, S. Haq: Hardware-aware automated quantization with mixed precision. In *Proceedings of the IEEE/CVF Conference on Computer Vision and Pattern Recognition (CVPR)*, 2019. URL [https://openaccess.thecvf.com/content\\_CVPR\\_2019/papers/Wang\\_HAQ\\_Hardware-Aware\\_Automated\\_Quantization\\_With\\_Mixed\\_Precision\\_CVPR\\_2019\\_paper.pdf](https://openaccess.thecvf.com/content_CVPR_2019/papers/Wang_HAQ_Hardware-Aware_Automated_Quantization_With_Mixed_Precision_CVPR_2019_paper.pdf).

Wang, S., Li, B. Z., Khabsa, M., Fang, H., and Ma, H. Linformer: Self-attention with linear complexity. *arXiv preprint arXiv:2006.04768*, 2020.

Wang, X., Yu, F., Dou, Z.-Y., Darrell, T., and Gonzalez, J. E. Skipnet: Learning dynamic routing in convolutional networks. In *Proceedings of the European Conference on Computer Vision (ECCV)*, 2018b. URL [https://openaccess.thecvf.com/content\\_ECCV\\_2018/html/Xin\\_Wang\\_SkipNet\\_Learning\\_Dynamic\\_ECCV\\_2018\\_paper.html](https://openaccess.thecvf.com/content_ECCV_2018/html/Xin_Wang_SkipNet_Learning_Dynamic_ECCV_2018_paper.html).

Wei, X., Gong, R., Liu, Y., Yu, F., Wang, W., Huang, J., Zhang, Q., and Gu, S. Qdrop: Randomly dropping quantization for extremely low-bit post-training quantization. *arXiv preprint arXiv:2203.05740*, 2022. URL <https://arxiv.org/abs/2203.05740>.

Weng, T.-W., Zhang, H., Chen, H., Song, Z., Hsieh, C.-J., Boning, D., Dhillon, I. S., and Daniel, L. Towards fast computation of certified robustness for ReLU networks. In *Proceedings of the 35th International Conference on Machine Learning (ICML)*, 2018. URL <https://arxiv.org/abs/1804.09699>.

Weng, T.-W., Zhao, P., Liu, S., Chen, P.-Y., Lin, X., and Daniel, L. Towards certificated model robustness against weight perturbations. In *Proceedings of the AAAI Conference on Artificial Intelligence (AAAI)*, 2020. URL <https://ojs.aaai.org/index.php/AAAI/article/view/6105/5961>.

Williams, A., Nangia, N., and Bowman, S. R. A broad-coverage challenge corpus for sentence understanding through inference. In *Proceedings of the 2018 Conference of the North American Chapter of the Association for Computational Linguistics: Human Language Technologies (NAACL-HLT)*, 2018. URL <https://aclanthology.org/N18-1101/>.

Williams, S., Waterman, A., and Patterson, D. Roofline: an insightful visual performance model for multicore architectures. *Communications of the ACM*, 52(4):65–76, 2009. doi: 10.1145/1498765.1498785.

Xiao, G., Lin, J., Seznec, M., Wu, H., Demouth, J., and Han, S. Smoothquant: Accurate and efficient post-training quantization for large language models. In *Proceedings of the 40th International Conference on Machine Learning (ICML)*, 2023. URL <https://proceedings.mlr.press/v202/xiao23c.html>.

Xiao, W., Bhardwaj, R., Ramjee, R., Sivathanu, M., Kwatra, N., Han, Z., Patel, P., Peng, X., Zhao, H., Zhang, Q., Yang, F., and Zhou, L. Gandiva: Introspective cluster scheduling for deep learning. In *13th USENIX Symposium on Operating Systems Design and Implementation (OSDI 18)*, pp. 595–610. USENIX Association, 2018.

Xu, S., Li, H., Zhuang, B., Liu, J., Cao, J., Liang, C., and Tan, M. Generative low-bitwidth data free quantization. In *European Conference on Computer Vision (ECCV)*, 2020. URL [https://www.ecva.net/papers/eccv\\_2020/papers\\_ECCV/papers/123570001.pdf](https://www.ecva.net/papers/eccv_2020/papers_ECCV/papers/123570001.pdf).

Yu, J. and Huang, T. Universally slimmable networks and improved training techniques. In *Proceedings of the IEEE/CVF International Conference on Computer Vision (ICCV)*, 2019. URL [https://openaccess.thecvf.com/content\\_ICCV\\_2019/papers/Yu\\_Universally\\_Slimmable\\_Networks\\_and\\_Improved\\_Training\\_Techniques\\_ICCV\\_2019\\_paper.pdf](https://openaccess.thecvf.com/content_ICCV_2019/papers/Yu_Universally_Slimmable_Networks_and_Improved_Training_Techniques_ICCV_2019_paper.pdf).

Yu, J., Yang, L., Xu, N., Yang, J., and Huang, T. Slimmable neural networks. In *International Conference on Learning Representations (ICLR)*, 2019. URL <https://openreview.net/forum?id=H1gMCsAqY7>.

Yu, P. and Chowdhury, M. Fine-grained gpu sharing primitives for deep learning applications. In *Proceedings of Machine Learning and Systems*, volume 2,

2020. URL [https://proceedings.mlsys.org/paper\\_files/paper/2020/hash/d9cd83bc91b8c36a0c7c0fccca59228f2-Abstract.html](https://proceedings.mlsys.org/paper_files/paper/2020/hash/d9cd83bc91b8c36a0c7c0fccca59228f2-Abstract.html).

Yuan, Z., Liu, J., Wu, J., Yang, D., Wu, Q., Sun, G., Liu, W., Wang, X., and Wu, B. Benchmarking the reliability of post-training quantization. *arXiv preprint arXiv:2303.13003*, 2023. URL <https://arxiv.org/abs/2303.13003>.

Zhang, H., Weng, T.-W., Chen, P.-Y., Hsieh, C.-J., and Daniel, L. Efficient neural network robustness certification with general activation functions. *Advances in neural information processing systems*, 31, 2018.

Zhang, P., Zeng, G., Wang, T., and Lu, W. Tinyllama: An open-source small language model. *arXiv preprint arXiv:2401.02385*, 2024. URL <https://arxiv.org/abs/2401.02385>.

Zhang, Q., Chen, M., Bukharin, A., Karampatziakis, N., He, P., Cheng, Y., Chen, W., and Zhao, T. Adalora: Adaptive budget allocation for parameter-efficient fine-tuning. *arXiv preprint arXiv:2303.10512*, 2023. URL <https://arxiv.org/abs/2303.10512>.

Zheng, L., Jia, C., Sun, M., Wu, Z., Yu, C. H., Haj-Ali, A., Wang, Y., Yang, J., Zhuo, D., Sen, K., Gonzalez, J. E., and Stoica, I. Ansor: Generating high-performance tensor programs for deep learning. In *14th USENIX Symposium on Operating Systems Design and Implementation (OSDI 20)*, 2020. URL <https://arxiv.org/abs/2006.06762>.

Zhou, A., Ma, Y., Zhu, J., Liu, J., Zhang, Z., Zhang, L., Zhu, W., and Huang, G. Learning n:m fine-grained structured sparse neural networks from scratch. In *International Conference on Learning Representations (ICLR)*, 2021. URL [https://openreview.net/forum?id=K9bw7vqp\\_s](https://openreview.net/forum?id=K9bw7vqp_s).

Zhou, S. et al. Dorefa-net: Training low bitwidth convolutional neural networks with low bitwidth gradients, 2016.

Zhou, Y., Liang, F., Chin, T.-W., and Marculescu, D. Play it cool: Dynamic shifting prevents thermal throttling. *arXiv preprint arXiv:2206.10849*, 2022. URL <https://arxiv.org/abs/2206.10849>.

## A. Extended Background & Related Work

### A.1 Expanded motivation & ecosystem needs

Modern ML deployment spans a jagged landscape of hardware, latency targets, and reliability constraints that change from hour to hour, user to user, and app to app; the same model may run in a multiplexed cloud service one minute, on a thermally throttled edge accelerator the next, and finally on a battery-constrained mobile CPU where memory bandwidth dominates FLOPs.(Xiao et al., 2018; Gu et al., 2019; Benoit-Cattin et al., 2020; Lin et al., 2023; Boroumand et al., 2021) In such settings, the dominant pain points arise from *rigidity of exported artifacts, budget uncertainty at runtime, and lack of dependable guardrails when compressing*.

First, classical pipelines materialize one compressed checkpoint per operating point (e.g., an 8-bit QAT model for server, a 4-bit PTQ variant for mobile, a pruned variant for an NPU). This multiplies storage, complicates A/B and rollback, fractures monitoring, and forces brittle routing logic that is sensitive to device idiosyncrasies and kernel availability. Second, real-world budgets are stochastic: co-tenancy and scheduler noise on GPUs, temperature and DVFS on edge devices, user-visible frame deadlines in interactive workloads, and on-device memory pressure that shifts with other applications. Operators therefore need *elasticity* at inference time: a knob that moves the model along the accuracy–latency–size frontier without retraining or re-exporting, and without violating hardware constraints (kernel shapes, quantization formats, alignment).

Third, production reliability increasingly demands *predictable failure modes*—particularly when compression trades accuracy for efficiency. SLAs and safety reviews ask not only “how fast” and “how accurate,” but “how far could the output shift when we trim 20% compute?” Today’s answers are empirical and often brittle; formal robustness work rarely translates into actionable deployment knobs, while many high-performing compression methods offer limited guarantees. The ecosystem trendlines intensify these pressures: model families are larger and more heterogeneous (CNNs, ViTs, MLP-Mixers, encoder/decoder LMs),(Dosovitskiy et al., 2021; Tolstikhin et al., 2021; Raffel et al., 2020) accelerators expose diverse datatypes (INT8, INT4, FP8, mixed per-channel schemes)(Micikevicius et al., 2022) and sparse/low-rank kernels that are highly vendor-specific,(Parashar et al., 2017) and privacy/latency requirements push more inference to the edge.

Operators need a *single, portable checkpoint* that can be *steered at test time* to hit budget targets on unfamiliar devices, with *monotone behavior* (a larger budget never hurts accuracy) and *telemetry hooks* that quantify risk. From a tooling viewpoint, the artifact should integrate with common export/compile steps (ONNX/TensorRT, mobile runtimes),(ONNX Community, 2017; NVIDIA, 2017) snap to discrete hardware profiles to avoid kernel gaps, and surface lightweight *certificates* that bound induced drift under admissible compressions. Finally, evaluation itself must evolve: heterogeneous-device Pareto curves with p50/p90 latencies, energy per inference, memory footprint including activation buffers, and *budget-respect rates* (how often a requested profile meets its latency/energy target) are as important as single-number accuracy.(Reddi et al., 2020) In short, the ecosystem needs compression that is *adaptive, certifiable, hardware-aware, and operationally simple*, converting compression from an offline engineering fork into an online control plane aligned with production SLOs.

### A.2 Detailed survey (quantization, pruning, low-rank, dynamic nets, verification)

**Quantization.** Post-training quantization (PTQ) calibrates scales/zero-points on a held-out set and is attractive for speed and simplicity, but its accuracy can degrade at ultra-low precision or under distribution shift; mitigations include per-channel scales, activation clipping, bias correction, and outlier-aware schemes that carve high-variance channels into higher precision. Quantization-aware training (QAT) replaces hard rounding with STE-based surrogates to learn scale/clipping parameters, generally improving robustness but at the cost of additional training and a fixed exported bit-width. Mixed-precision methods cast bit allocation as a search or differentiable relaxation (reward/gradients from latency proxies) to distribute bits across layers; deployment friction arises when the chosen mix does not map cleanly to vendor kernels, necessitating profile pruning. Recent PTQ/QAT hybrids add knowledge distillation and cross-layer equalization; they push the pareto frontier but still *freeze* precision at export and provide no explicit bound on output drift.(Choi et al., 2018; Nagel et al., 2019; Zhou et al., 2016; Dong et al., 2019; Lou et al., 2019; Frantar et al., 2022)

**Pruning and sparsity.** Unstructured pruning achieves high parameter sparsity and small on-disk size, but real speedups require fine-grained sparse kernels with nontrivial overheads; structured or channel pruning yields reliable latency gains by shrinking whole filters/projections, though it often needs iterative re-training and careful schedules to avoid accuracy cliffs. Movement- and magnitude-based criteria, L0/L1 relaxations, and lottery-ticket style rewinds populate the design space; dynamic sparsity adds input adaptivity but complicates compilation and predictability.(Han et al., 2015a; Luo et al., 2017;

Lee et al., 2018; Frankle & Carbin, 2018; Louizos et al., 2017; Evci et al., 2020)

**Low-rank and tensor factorization.** SVD/Tucker/CP decompositions reduce parameters and memory traffic in dense and convolutional layers; in Transformers, factorizations applied to projection matrices and MLP blocks trade rank for accuracy. LoRA-style adapters inject low-rank updates during fine-tuning, and low-rank *replacement* compresses the base weights; most approaches fix rank offline and re-export per rank, which clashes with runtime adaptivity and kernel availability. Joint rank-precision allocation is comparatively underexplored: quantization interacts with rank because truncation changes dynamic ranges and singular spectra, which in turn affects scale selection and error propagation.(Novikov et al., 2015; Wang et al., 2020; Dettmers et al., 2023)

**Dynamic networks.** Early exiting, token/channel dropping, and input-conditional routing tailor compute to difficulty, improving average latency. However, they require architectural hooks, retraining, and careful calibration to avoid pathological exits; guarantees are typically statistical (expected cost) rather than *per-budget* deterministic. Moreover, dynamic policies can adversarially interact with batching, caching, or compiler fusions, yielding unstable tail latencies.(Huang et al., 2017; Rao et al., 2021; Fedus et al., 2022)

**Verification and certificates.** Robustness certificates bound output change under input or parameter perturbations (e.g., Lipschitz, interval/zonotope bounds, randomized smoothing). Parameter-perturbation guarantees—relevant for compression—bound the effect of quantization noise, pruning, or low-rank truncation, but many are conservative or expensive to compute at scale, and few are wired into a deployment-time control loop. Practical adoption is hindered by the gap between math-friendly assumptions and production details like residual connections, normalization, fused kernels, and calibration drift.(Zhang et al., 2018; Cohen et al., 2019; Weng et al., 2018)

**Positioning.** Against this backdrop, a practical method should: 1) *train once* yet expose a *continuous* control that snaps to *discrete hardware profiles* at inference; 2) *jointly* reason about rank and precision because their errors compound and their costs couple to memory bandwidth and kernel shapes; 3 provide a *fast, layerwise certificate* that upper-bounds logit drift for the selected profile and can be surfaced to monitoring; and (iv) preserve *monotonicity in budget* so operators can raise a target without risking accuracy regressions. The prevailing literature supplies powerful pieces—accurate PTQ/QAT at fixed bits, effective pruning schedules, strong low-rank adapters, and rigorous but heavy certificates—but rarely assembles them into an elastic, certifiable, and hardware-conscious pipeline that speaks the language of production SLOs. T3C is designed to bridge this gap by sharing parameters across ranks, tying bit-width to rank in a deployable way, and attaching a certificate that is cheap enough for training-time regularization and export-time reporting, thereby turning compression into an operational control rather than an offline fork.

## B. Method Details

### B.1 Notation & tensor decompositions (SVD/Tucker/CP variants)

**Basic notation.** We consider a feed-forward network with layers indexed by  $\ell \in \{1, \dots, L\}$ . For a dense (fully-connected) layer  $\ell$ , let  $W_\ell \in \mathbb{R}^{m_\ell \times n_\ell}$  map  $a_{\ell-1} \in \mathbb{R}^{n_\ell}$  to  $h_\ell = W_\ell a_{\ell-1}$  (biases omitted for brevity); activations may include normalization and nonlinearity  $h_\ell \mapsto a_\ell$ . For a convolutional kernel,  $W_\ell \in \mathbb{R}^{C_{\text{out}} \times C_{\text{in}} \times h \times w}$  uses stride/padding as in the base model. Given input  $x$ , the full model produces logits  $z = f(x)$ ; under a budget profile  $k$  with per-layer rank/bit  $(k_\ell, q_\ell)$ , we denote the compressed model by  $\tilde{f}_k(x)$  with logits  $\tilde{z}$ .

**SVD (matrix) factorization.** For  $W \in \mathbb{R}^{m \times n}$ , the rank- $r$  truncated SVD is  $W_r = U_{:,1:r} \Sigma_{1:r} V_{:,1:r}^\top$  with singular values  $\sigma_1 \geq \dots \geq \sigma_r$ . We maintain factors up to  $k_{\max}$  and expose a differentiable top- $k \leq k_{\max}$  selection (Sec. B.2). We employ two numerically stable parameterizations: (i) *spectral form*  $U, \Sigma, V$  with orthogonality constraints enforced by implicit re-orthogonalization via Householder updates; (ii) *product form*  $AB^\top$ ,  $A \in \mathbb{R}^{m \times k_{\max}}$ ,  $B \in \mathbb{R}^{n \times k_{\max}}$ , with a spectral penalty encouraging  $A$  and  $B$  to approximate singular directions. Spectral form yields direct control of the residual norm  $\|W - W_k\|_2 = \sigma_{k+1}$  and  $\|W - W_k\|_F = (\sum_{i>k} \sigma_i^2)^{1/2}$ , useful for certificates.

**Tucker-2 for convolution.** For  $W \in \mathbb{R}^{C_o \times C_i \times h \times w}$  we use channel-only Tucker-2:

$$W \approx (U_o, U_i) \cdot G, \quad U_o \in \mathbb{R}^{C_o \times r_o}, U_i \in \mathbb{R}^{C_i \times r_i}, G \in \mathbb{R}^{r_o \times r_i \times h \times w}. \quad (9)$$

The effective forward is  $\text{Conv}(U_o \text{Conv}(G, U_i^\top \cdot))$ , which compiles to three kernels (pointwise  $1 \times 1$ , spatial  $h \times w$ , pointwise  $1 \times 1$ ). Budget  $k$  maps to  $(r_o(k), r_i(k))$  via a monotone schedule.

**CP for depthwise/attention blocks.** For depthwise-like or MLP projection weights with strong separability, a CP rank- $r$  factorization  $W \approx \sum_{j=1}^r a_j^{(1)} \otimes a_j^{(2)}$  reduces memory traffic; in attention, we optionally share a single  $k$  across  $\{W_Q, W_K, W_V, W_O\}$  to avoid head imbalance.

**Identifiability and conditioning.** Tucker and CP are non-unique up to scale/permuation. We eliminate degeneracies with per-factor  $\ell_2$  normalization and a permutation-fixing rule (descending factor norms). To prevent ill-conditioning at small ranks, we regularize the spectrum by  $\sum_i \max(0, \sigma_i - \sigma_{i+1} - \delta)$  to keep gaps from collapsing (small  $\delta$ ).

## B.2 Loss terms, annealing schedules, $\lambda$ sweeps

**Total objective (expanded).** For a minibatch  $\mathcal{B}$  and sampled budget profile  $k$ , the loss is

$$\mathcal{L} = \underbrace{\frac{1}{|\mathcal{B}|} \sum_{(x,y) \in \mathcal{B}} \text{CE}(f_{\text{full}}(x), y)}_{\text{task (full)}} + \lambda_{\text{SD}} \underbrace{\frac{1}{|\mathcal{B}|} \sum_{x \in \mathcal{B}} \text{KL}(p_{\text{full}}(x) \| p_k(x))}_{\text{self-distill}} + \lambda_{\text{AUG}} \underbrace{\mathbb{E}_{\tilde{x} \sim \mathcal{T}(x)} \text{KL}(p_{\text{full}}(\tilde{x}) \| p_k(\tilde{x}))}_{\text{augmentation consistency}} + \lambda_{\text{CERT}} \underbrace{\max(0, \hat{\Delta}(k) - \epsilon)}_{\text{certificate penalty}} + \lambda_{\text{BUD}} \underbrace{\text{Cost}(k; b)}_{\text{budget proxy}}, \quad (10)$$

with  $p(\cdot) = \text{softmax}(z/T)$  (temperature  $T=1$  unless specified). The *task (full)* term trains the high-rank view ( $k=k_{\max}$  or a high-rank proxy), anchoring teacher quality. The two KL terms align compressed predictions to the full model on raw and lightly augmented inputs. The certificate penalty uses the bound from Sec. 4 (main paper) with running estimates. The budget proxy is the expected normalized latency/energy/size against a target.

**Annealing schedules.** *Top- $k$  temperature.* For the Gumbel-Top- $k$  mask logits  $g_i$ , we use temperature  $\tau_t = \max(\tau_{\min}, \tau_0 \cdot \gamma^{t/T_{\text{anneal}}})$  with  $\gamma \in (0, 1)$ , annealed over  $T_{\text{anneal}}$  steps, then held. *Rank sampling.* Early curriculum: sample  $k$  from a wide Beta( $\alpha=0.75, \beta=0.75$ ) on  $[k_{\min}, k_{\max}]$ , then bias toward deployment-relevant profiles by mixing a categorical over discrete profiles  $\{k^{(j)}\}_j$ . *Coefficient ramps.* We use linear warmups for  $\lambda_{\text{SD}}, \lambda_{\text{AUG}}, \lambda_{\text{CERT}}$  over the first 10–20% of training to avoid early over-regularization.

**$\lambda$  sweeps and stability.** We recommend a coarse-to-fine sweep: fix  $\lambda_{\text{BUD}}$  to meet a target utilization (latency/energy) on the validation device, then search  $\lambda_{\text{CERT}}$  to cap violation rates (fraction of samples where  $\hat{\Delta}(k) > \epsilon$ ), and finally tune  $\lambda_{\text{SD}}$  and  $\lambda_{\text{AUG}}$  to recover accuracy at tight budgets. In practice, a good starting box is

$$\lambda_{\text{SD}} \in [0.3, 1.0], \quad \lambda_{\text{AUG}} \in [0.1, 0.5], \quad \lambda_{\text{CERT}} \in [0.05, 0.5], \quad \lambda_{\text{BUD}} \in [0.1, 1.0]. \quad (11)$$

We monitor (i) monotonicity (accuracy should be non-decreasing in budget), (ii) % budget violations, and (iii) calibration error between  $\hat{\Delta}(k)$  and observed drift.

## B.3 Quantizer definitions, calibration, rounding tricks

**Uniform affine quantization.** For a real tensor  $T$ ,  $q$ -bit symmetric per-tensor quantization uses scale  $s > 0$  and integer grid  $\mathcal{G}_q = \{-2^{q-1} + 1, \dots, 2^{q-1} - 1\}$ :

$$\text{Quantize}_q(T) = s \text{clip}\left(\left\lfloor \frac{T}{s} \right\rfloor, \min \mathcal{G}_q, \max \mathcal{G}_q\right), \quad s = \frac{\max(|T|)}{2^{q-1} - 1}. \quad (12)$$

We also use per-channel scales  $s_c$  for matrices along output channels (rows) and for conv along  $C_{\text{out}}$ .

**Straight-through estimator (STE).** In backprop, we treat  $\partial[u]/\partial u \approx 1$  inside the clipping range and 0 outside. For scale  $s$ , we learn  $s$  (log-parameterized) with gradient  $\frac{\partial \text{Quantize}_q(T)}{\partial s} \approx (|T/s| - T/s)$  inside range, encouraging scale to match the signal range.

**Rounding variants.** *Stochastic rounding*  $\lfloor u \rfloor_{\text{stoch}} = \lfloor u \rfloor$  with prob  $1 - (u - \lfloor u \rfloor)$  else  $\lceil u \rceil$ , used at training-time to reduce bias at low  $q$ ; disabled at export for determinism. *Bias correction* adds a folded offset  $\delta = \mathbb{E}[T - \text{Quantize}_q(T)]$  (per-channel) to the dequantized tensor during calibration and is then fused into bias parameters. *Outlier-aware splitting* routes a small fraction  $\rho$  of largest-magnitude channels to  $q + \Delta q$  bits when hardware supports mixed precision within a layer; we expose this as a profile option so the controller can assign higher bits to outlier groups.

**Calibration.** We compute  $s$  (and optionally zero-point for asymmetric quantization) from a calibration set  $\mathcal{C}$  via either: (i) *max-range* (as above), or (ii) *percentile clipping*  $s = \text{percentile}_p(|T|)/(2^{q-1} - 1)$  with  $p \in [99.0, 99.99]$  tuned to minimize validation KL between float and quantized outputs of the layer. We maintain EMA statistics of  $s$  during training to stabilize deployment scales.

**Rank-tied bit allocation.** We use a monotone map  $q(k) = \min\{q_{\max}, \lfloor a \log k + b \rfloor\}$  per factor group with small per-factor offsets (e.g.,  $q_U = q(k) + 1$ ,  $q_G = q(k)$ ,  $q_V = q(k) + 1$ ) ensuring higher rank receives at least as many bits. This interacts favorably with spectral decay: smaller ranks truncate more energy and benefit less from extra precision.

**Lemma (expected dequantization error under stochastic rounding).** Let  $X$  be a scalar with  $|X| \leq M$  and fixed scale  $s$ . With stochastic rounding on the grid  $s\mathcal{G}_q$  and no clipping, the dequantization error  $\varepsilon = \text{Quantize}_q(X) - X$  satisfies  $\mathbb{E}[\varepsilon | X] = 0$  and  $\text{Var}(\varepsilon | X) \leq s^2/4$ . *Proof.* Conditioning on  $u = X/s$ , the rounding picks  $\lfloor u \rfloor$  with prob  $1 - (u - \lfloor u \rfloor)$  and  $\lceil u \rceil$  otherwise; the expectation equals  $u$ . Multiply by  $s$  to get unbiasedness; the conditional variance of a Bernoulli with step size  $s$  is bounded by  $s^2/4$ .  $\square$

#### B.4 Controller architectures & training (relaxations, baselines)

**Budget tokenization.** A budget  $b$  encodes target latency/energy/size and optionally a device id. We embed  $b$  as  $e_b = \text{Embed}_{\text{dev}}(\text{id}) \oplus \phi(\text{lat, energy, size})$  where  $\phi$  is a learned MLP on normalized scalars;  $\oplus$  denotes concatenation.

**Policy head.** We use a shared two-layer MLP  $\pi_\phi$  that outputs per-layer logits for discrete profiles and, optionally, a continuous proposal projected onto those profiles:

$$\hat{k}_\ell, \hat{q}_\ell = \text{Proj}(W_2 \sigma(W_1[e_b \oplus s(x)])), \quad \text{Proj} : \mathbb{R}^2 \rightarrow \mathcal{P}_\ell \subset \{(k, q)\}. \quad (13)$$

Here  $s(x)$  is an optional input summary (e.g., pooled penultimate activations averaged over the batch).  $\mathcal{P}_\ell$  is a layer-specific menu of hardware-aligned  $(k, q)$  pairs.

**Discrete relaxations.** We use Gumbel-Softmax over  $\mathcal{P}_\ell$  with temperature  $\tau$  and the straight-through trick to obtain a one-hot (profile index) in the forward pass and a soft distribution in the backward pass. This preserves end-to-end differentiability while training the controller jointly with factors and quantizers.

**Training objectives for the controller.** The controller is trained implicitly by the total loss (Eq. 10); gradients propagate through the differentiable relaxation and the budget/certificate penalties. When using purely discrete selection (no relaxation), we add a REINFORCE term:

$$\nabla_\phi \mathbb{E}_{\pi_\phi} [-\mathcal{L}] \approx \mathbb{E}[(-\mathcal{L} - b) \nabla_\phi \log \pi_\phi], \quad (14)$$

with a learned baseline  $b$  (value head) to reduce variance. In practice, the Gumbel-Softmax + straight-through suffices, switching to pure argmax after the anneal.

**Monotonicity enforcement.** We ensure that higher budgets cannot yield smaller ranks/bits via isotonic constraints: for two budget tokens  $b_1 \prec b_2$  (componentwise), we add a hinge

$$\lambda_{\text{ISO}} \sum_\ell \max(0, k_\ell(b_1) - k_\ell(b_2)) + \max(0, q_\ell(b_1) - q_\ell(b_2)). \quad (15)$$

At export, we drop any violating profiles and re-calibrate the remaining set to keep the partial order.

**Baselines (for ablations).** (i) **Rank-only**:  $q$  fixed per layer; (ii) **Bit-only**: fixed ranks; (iii) **Greedy knapsack**: allocate  $k/q$  to layers in order of benefit/cost ratio using measured latency tables; (iv) **Uniform**: same  $k, q$  across layers. These illustrate the value of joint learning and the controller’s allocation.

## B.5 Algorithmic complexity & memory analysis per layer type

Let  $b_w$  be weight bit-width,  $b_a$  activation bit-width at inference (often 8), and denote by  $\mathcal{B}(\cdot)$  the bytes footprint. We separate *compute FLOPs* and *memory bytes* (weights + activation reads/writes), as the latter dominates on many edge devices.

**Dense layer**  $W \in \mathbb{R}^{m \times n}$ . *Full* GEMV FLOPs (batch 1) and weight bytes:

$$\text{FLOPs}_{\text{full}} = 2mn, \quad \mathcal{B}_W = mn \cdot \frac{b_w}{8}. \quad (16)$$

*Rank- $k$  SVD path:* compute as  $(U_{m \times k} \Sigma_{k \times k} V_{n \times k}^\top) a$  via  $(V^\top a) \in \mathbb{R}^k$ , multiply by  $\Sigma$ , then  $U$ :

$$\text{FLOPs}_{\text{SVD}}(k) \approx 2nk + k + 2mk \approx 2(n + m)k. \quad (17)$$

Weights bytes (per-factor; replace  $b_w$  by  $q(k)$  for mixed precision):

$$\mathcal{B}_U = mk \cdot \frac{b_w}{8}, \quad \mathcal{B}_V = nk \cdot \frac{b_w}{8}, \quad \mathcal{B}_\Sigma = k \cdot \frac{b_w}{8}. \quad (18)$$

**Convolution (Tucker-2).** Let the feature-map spatial size be  $H \times W$ . *Full* conv FLOPs:

$$\text{FLOPs}_{\text{full}} = 2C_o C_i h w H W. \quad (19)$$

*Tucker-2* as (reduce  $1 \times 1$ )  $\rightarrow$  (spatial)  $\rightarrow$  (expand  $1 \times 1$ ):

$$\text{FLOPs}_{\text{Tucker2}}(r_o, r_i) = 2H W \left( C_i r_i + r_o r_i h w + C_o r_o \right). \quad (20)$$

Weight bytes with rank-tied  $q = q(k)$ :

$$\mathcal{B}_{U_o} = C_o r_o \cdot \frac{q}{8}, \quad \mathcal{B}_{U_i} = C_i r_i \cdot \frac{q}{8}, \quad \mathcal{B}_G = r_o r_i h w \cdot \frac{q}{8}. \quad (21)$$

**Attention projections and MLP.** With  $d_{\text{model}}=d$  and MLP hidden  $d_{\text{ff}}$ , four projections  $W_Q, W_K, W_V, W_O \in \mathbb{R}^{d \times d}$  and  $W_1 \in \mathbb{R}^{d_{\text{ff}} \times d}$ ,  $W_2 \in \mathbb{R}^{d \times d_{\text{ff}}}$ . Applying SVD rank- $k$  to a  $d \times d$  matmul yields the rough FLOPs scaling:

$$\frac{\text{FLOPs}_{\text{rank-}k}}{\text{FLOPs}_{\text{full}}} \simeq \frac{2dk}{2d^2} = \frac{k}{d}. \quad (22)$$

**Latency/energy proxy (per device calibration).**

$$\widehat{\text{Lat}}(k) = \alpha_0 + \sum_{\ell=1}^L \left( \alpha_\ell^{\text{comp}} \cdot \text{FLOPs}_\ell(k) + \alpha_\ell^{\text{mem}} \cdot \text{Bytes}_\ell(k) \right), \quad (23)$$

with coefficients fitted by least squares on a grid of profiles. An analogous  $\widehat{\text{Energy}}(k)$  uses its own coefficients.

**Certificate aggregation cost.** Per layer, maintain: (i)  $\hat{L}_\ell$  via  $s$  power iterations; (ii) residual spectral norm  $\|\Delta W_\ell(k)\|_2$  via 1–2 PIs; (iii) activation RMS  $\alpha_\ell$  via EMA. Aggregate:

$$\hat{\Delta}(k) = \sum_{\ell=1}^L \hat{L}_\ell \|\Delta W_\ell(k)\|_2 \alpha_\ell. \quad (24)$$

**When does rank- $k$  win (threshold analysis)?** GEMV-like inference benefits from SVD when

$$2(n + m)k \ll 2mn \implies k \ll \frac{mn}{m + n}. \quad (25)$$

For square  $m=n=d$ :

$$k \ll \frac{d}{2} \quad (\text{compute-only; bandwidth effects tighten this bound}). \quad (26)$$

For conv Tucker-2, require

$$C_i r_i + r_o r_i h w + C_o r_o \ll C_o C_i h w. \quad (27)$$

Setting  $r_o = \rho C_o$ ,  $r_i = \rho C_i$  gives

$$\rho(C_i + C_o) + \rho^2 C_o C_i h w \ll C_o C_i h w \quad \Rightarrow \quad \rho \ll 1 \text{ and } \rho \lesssim \frac{1}{\sqrt{h w}}. \quad (28)$$

**Memory summaries.** Rank- $k$  SVD (bytes):

$$\mathcal{B}_W^{\text{SVD}}(k) \approx (mk + nk + k) \cdot \frac{q(k)}{8}. \quad (29)$$

Tucker-2 (bytes):

$$\mathcal{B}_W^{\text{T2}}(r_o, r_i) \approx (C_o r_o + C_i r_i + r_o r_i h w) \cdot \frac{q(k)}{8}. \quad (30)$$

**Proposition (monotone budget  $\Rightarrow$  non-increasing proxy cost).** If each layer's profile set  $\mathcal{P}_\ell$  is totally ordered so that  $(k', q') \succeq (k, q)$  implies  $\text{FLOPs}_\ell(k', q') \geq \text{FLOPs}_\ell(k, q)$  and  $\text{Bytes}_\ell(k', q') \geq \text{Bytes}_\ell(k, q)$ , and the controller enforces  $b_1 \prec b_2 \Rightarrow (k_\ell, q_\ell)(b_1) \preceq (k_\ell, q_\ell)(b_2)$  for all  $\ell$ , then

$$\widehat{\text{Lat}}(b_1) \leq \widehat{\text{Lat}}(b_2). \quad (31)$$

*Proof sketch.* Linearity of  $\widehat{\text{Lat}}$  in non-negative coefficients and per-layer monotonicity preserve the partial order when summed over layers.  $\square$

**Computational overhead of T3C versus fixed compression.** Training adds (i) factorized forward, (ii) STE quantization ops, (iii) a few PI steps per block intermittently. Empirically,

$$\text{Overhead}_{\text{train}} \approx (1.1 \text{ to } 1.4) \times \text{QAT wall-clock}, \quad (32)$$

amortized across all ranks/budgets since no re-training per operating point is needed.

## C. Certificates & Proofs

### C.1 Formal assumptions (Lipschitz proxies, normalization)

We formalize the network and the mild regularity needed for the certificate.

**Network and perturbation model.** Let  $f : \mathbb{R}^{d_0} \rightarrow \mathbb{R}^{d_L}$  be a feed-forward network of  $L$  blocks. Each block

$$h_\ell = \Phi_\ell(h_{\ell-1}; W_\ell), \quad \ell = 1, \dots, L, \quad h_0 \equiv x, \quad (33)$$

may be (i) an affine layer  $h \mapsto W_\ell h + b_\ell$  followed by a pointwise nonlinearity, (ii) a conv/attn block with residuals, or (iii) a normalization  $N_\ell$  with fixed (eval-mode) statistics. Let  $\tilde{f}_k$  be the *compressed* network obtained by replacing  $W_\ell$  with  $\tilde{W}_\ell(k)$  (e.g., rank/bit profile indexed by  $k$ ). Define per-layer residuals

$$\Delta W_\ell(k) := W_\ell - \tilde{W}_\ell(k). \quad (34)$$

**Post-layer Jacobian gains.** For each layer  $\ell$ , denote by  $T_{\ell \rightarrow L}$  the *post-layer* mapping that takes the input at layer  $\ell$  (i.e.,  $h_\ell$ ) to the logits  $z \in \mathbb{R}^{d_L}$  when all *subsequent* blocks are kept fixed. Its Jacobian operator norm is

$$L_\ell^*(x) := \left\| J_{T_{\ell \rightarrow L}}(h_\ell(x)) \right\|_2. \quad (35)$$

In practice we estimate a *proxy*  $\hat{L}_\ell$  by a few power-iteration steps on an efficient linearization; we assume a bounded slack  $\eta_\ell \geq 1$  such that

$$L_\ell^*(x) \leq \hat{L}_\ell \leq \eta_\ell L_\ell^*(x), \quad \text{uniformly over } x \in \mathcal{C}. \quad (36)$$

**Blockwise Lipschitzness and normalization.** For each block, the map  $u \mapsto \Phi_\ell(u; W_\ell)$  is  $L_\Phi$ -Lipschitz in  $u$  and  $L_{W,\ell}$ -smooth in  $W_\ell$  locally around  $(h_{\ell-1}, W_\ell)$ :

$$\|\Phi_\ell(u; W_\ell) - \Phi_\ell(v; W_\ell)\|_2 \leq L_{\Phi,\ell} \|u - v\|_2, \quad \|\Phi_\ell(h_{\ell-1}; W_\ell) - \Phi_\ell(h_{\ell-1}; \tilde{W}_\ell)\|_2 \leq L_{W,\ell} \|W_\ell - \tilde{W}_\ell\|_2 \|h_{\ell-1}\|_2. \quad (37)$$

For affine  $\rightarrow$  pointwise blocks with 1-Lipschitz activations (ReLU/GELU approximated near-linear region),  $L_{\Phi,\ell} \leq \|W_\ell\|_2$  and  $L_{W,\ell} \leq 1$  (by submultiplicativity). Normalization layers used in *eval mode* (e.g., frozen BatchNorm, LayerNorm with fixed  $\gamma, \beta$ ) are treated as fixed linear-affine transforms with operator gain  $L_{N,\ell}$  absorbed into  $L_{\Phi,\ell}$ .

**Residual connections.** For a residual block  $h_\ell = h_{\ell-1} + \Psi_\ell(h_{\ell-1}; W_\ell)$  with  $\Psi_\ell$   $L_{\Psi,\ell}$ -Lipschitz, the post-layer gain satisfies

$$L_{\ell-1}^*(x) \leq (1 + L_{\Psi,\ell}) L_\ell^*(x). \quad (38)$$

In our certificate we *do not* multiply residual gains; we push all post-layer amplification into  $L_\ell^*$  via direct Jacobian estimation.

## C.2 Full proof of the logit-drift bound (layerwise $\rightarrow$ network)

We bound  $\delta z(x; k) := \tilde{f}_k(x) - f(x)$  by *layer-local* perturbations propagated through post-layer Jacobians.

**One-layer replacement bound.** Fix  $x$  and some  $\ell$ . Consider the hybrid network  $f^{(\ell)}$  that uses  $\tilde{W}_\ell(k)$  only at layer  $\ell$  and  $W_j$  elsewhere. Let  $h_{\ell-1}$  be the pre- $\ell$  activation in  $f$  (and also in  $f^{(\ell)}$ , since layers  $< \ell$  match). The activation change at layer  $\ell$  is

$$\Delta h_\ell := \Phi_\ell(h_{\ell-1}; \tilde{W}_\ell) - \Phi_\ell(h_{\ell-1}; W_\ell). \quad (39)$$

By the  $W$ -smoothness,

$$\|\Delta h_\ell\|_2 \leq L_{W,\ell} \|\tilde{W}_\ell - W_\ell\|_2 \|h_{\ell-1}\|_2. \quad (40)$$

Propagating this change through subsequent layers  $\ell+1, \dots, L$  gives the logit difference

$$\delta z^{(\ell)}(x; k) := f^{(\ell)}(x) - f(x) = T_{\ell \rightarrow L}(h_\ell + \Delta h_\ell) - T_{\ell \rightarrow L}(h_\ell). \quad (41)$$

By the mean-value form (or Lipschitzness of  $T_{\ell \rightarrow L}$  around  $h_\ell$ ),

$$\|\delta z^{(\ell)}(x; k)\|_2 \leq L_\ell^*(x) \|\Delta h_\ell\|_2 \leq L_\ell^*(x) L_{W,\ell} \|\Delta W_\ell(k)\|_2 \|h_{\ell-1}\|_2. \quad (42)$$

**Layerwise telescoping via triangle inequality.** Build the fully compressed network by replacing layers one at a time:

$$f \xrightarrow{\ell=1} f^{(1)} \xrightarrow{\ell=2} f^{(2)} \xrightarrow{\dots} f^{(L)} = \tilde{f}_k. \quad (43)$$

Then

$$\tilde{f}_k(x) - f(x) = \sum_{\ell=1}^L (f^{(\ell)}(x) - f^{(\ell-1)}(x)), \quad f^{(0)} := f, \quad (44)$$

and by the triangle inequality together with (42),

$$\|\delta z(x; k)\|_2 \leq \sum_{\ell=1}^L L_\ell^*(x) L_{W,\ell} \|\Delta W_\ell(k)\|_2 \|h_{\ell-1}(x)\|_2. \quad (45)$$

**Practical proxy and certificate statement.** Absorb  $L_{W,\ell}$  into  $L_\ell^*(x)$  (it equals 1 for affine  $\rightarrow$  pointwise with 1-Lipschitz nonlinearity), and replace  $L_\ell^*(x)$  by its proxy  $\hat{L}_\ell$  (estimated via power iteration). This yields the deployable bound

$$\|\delta z(x; k)\|_2 \leq \sum_{\ell=1}^L \hat{L}_\ell \|\Delta W_\ell(k)\|_2 \|a_{\ell-1}(x)\|_2,$$

(46)

with  $a_{\ell-1} \equiv h_{\ell-1}$  the input to layer  $\ell$ . This is the claimed *pointwise* logit-drift certificate.

### C.3 Data-dependent tightening via activation norms

We now derive an *expected* (dataset-calibrated) certificate that is often tighter and more stable.

**Calibration statistics and Jensen/Cauchy–Schwarz.** Let  $\mathcal{C}$  be a calibration set. Define per-layer activation RMS

$$\alpha_\ell := \left( \mathbb{E}_{x \in \mathcal{C}} \|a_{\ell-1}(x)\|_2^2 \right)^{1/2}. \quad (47)$$

Square both sides of (46), apply Jensen’s inequality and then Cauchy–Schwarz on each summand to obtain

$$\left( \mathbb{E}_{x \in \mathcal{C}} \|\delta z(x; k)\|_2^2 \right)^{1/2} \leq \sum_{\ell=1}^L \hat{L}_\ell \|\Delta W_\ell(k)\|_2 \left( \mathbb{E}_{x \in \mathcal{C}} \|a_{\ell-1}(x)\|_2^2 \right)^{1/2}. \quad (48)$$

Thus,

$$\left( \mathbb{E}_{x \in \mathcal{C}} \|\delta z(x; k)\|_2^2 \right)^{1/2} \leq \sum_{\ell=1}^L \hat{L}_\ell \|\Delta W_\ell(k)\|_2 \alpha_\ell = \hat{\Delta}(k).$$

(49)

Because  $\alpha_\ell$  reflects the *typical* activation energy for in-distribution inputs, (49) tightens (46) whenever activations exhibit non-adversarial variability. At deploy time we report quantiles of  $\hat{\Delta}(k)$  across  $\mathcal{C}$ .

**Remark on residual/normalization stacking.** The proof above does *not* require multiplying per-layer Lipschitz constants across the entire network. All post-layer amplification is contained in  $\hat{L}_\ell$ , which is *directly* estimated at the operating point (architecture, normalization, residual topology), yielding tighter—and empirically stable—bounds.

### C.4 Counterexamples & tightness discussion

**(1) Heavy-tailed activations  $\Rightarrow$  loose pointwise bound.** Consider a single affine layer  $z = Wa$  with ReLU upstream producing heavy-tailed  $\|a\|_2$ . Even if  $\|\Delta W\|_2$  is small, the product  $\|\Delta W\|_2 \|a\|_2$  can be large with non-negligible probability, making the *pointwise* bound (46) loose. The *expected* form (49) mitigates this by replacing  $\|a\|_2$  with  $\alpha$ , but will still reflect any genuine heavy tails. *Tightening*: activation clipping or norm-aware regularization reduces  $\alpha$ ; weight normalization can reduce  $\hat{L}_\ell$ .

**(2) Input-dependent normalization.** BatchNorm in *train mode* depends on the batch and is not globally Lipschitz w.r.t. input in a data-independent way. Our certificate assumes eval-mode statistics (fixed affine map), otherwise  $L_\ell^*$  can spike. *Tightening*: freeze BN (eval mode) during certification; estimate  $\hat{L}_\ell$  under the exact deploy graph.

**(3) Attention with sharp softmax.** Self-attention contains  $\text{softmax}(QK^\top / \sqrt{d})V$ . The Jacobian of softmax has operator norm bounded but can approach 1 as logits flatten; coupled with large  $\|Q\|_2 \|K\|_2$ ,  $L_\ell^*$  may be large. *Tightening*: temperature regularization or spectral control (e.g., weight scaling) to bound  $Q, K$ ; estimate  $\hat{L}_\ell$  after such rescaling.

**(4) Non-Lipschitz blocks by construction.** If a block explicitly amplifies norms, e.g.,  $h \mapsto \gamma h$  with  $\gamma \gg 1$  inside a residual branch without compensation, then even tiny  $\|\Delta W\|_2$  can induce large drift. Our estimate  $\hat{L}_\ell$  will correctly reflect this; the certificate is loose only if  $\hat{L}_\ell$  is underestimated. *Tightening*: conservative power-iteration (more steps), residual scaling, or spectral normalization.

**(5) Quantization mismatch.** Certificates are computed for the *inference* graph. If training uses STE and deploy uses integer kernels with different rounding/saturation, then  $\Delta W_\ell$  measured in float may underestimate effective perturbation. *Tightening*: compute  $\|\Delta W_\ell\|_2$  on *dequantized* tensors produced by the exact kernels; incorporate per-tensor scale/zero-point in the operator.

**Global tightness comment.** The bound (45) is *first-order tight* for networks where subsequent blocks are locally well-approximated by linear maps around  $h_\ell(x)$ ; any nonlinearity curvature introduces second-order residuals that our estimator ignores, making the bound conservative (safe). Empirically, by (i) measuring  $\hat{L}_\ell$  at the deploy graph, (ii) using data-dependent  $\alpha_\ell$ , and (iii) focusing on spectral-norm residuals of the *compressed operator*, we obtain a certificate that correlates well with observed drift while remaining computationally light.

**Summary of the guarantee.** Under the stated assumptions, the pointwise and expected certificates (46)–(49) hold. Violations can occur only if the proxy  $\hat{L}_\ell$  underestimates the true post-layer gain or if the deploy graph differs from the certified one; both are addressed by conservative estimation (extra power iterations) and certifying *exact* runtime kernels.

## D. Deployment & Engineering

### D.1 Kernel choices (GEMM vs tensor-core paths; layout)

**Operator mapping.** Each factorized operator must be lowered to a concrete kernel that respects datatype, tile granularity, and memory layout. For SVD-style layers we realize  $\tilde{W}(k) = U_{m \times k} \Sigma_{k \times k} V_{n \times k}^\top$  as two GEMMs with an inexpensive diagonal scaling, while Tucker-2 uses a sequence  $1 \times 1$  reduce  $\rightarrow$  spatial core  $\rightarrow 1 \times 1$  expand. We adhere to three regimes:

- **Scalar-GEMM paths** (CPU/older GPU): robust for skinny inner dimensions  $k \ll \min(m, n)$ , portable across FP32/FP16/INT8. Favor these when tensor-core tiles would be grossly underutilized.
- **Tensor-core MMA paths** (modern GPU/NPU): best throughput if the contracting dimension and leading dimensions align with native tile multiples (e.g., 8, 16, or 32 depending on dtype). When  $k$  is small, group multiple independent contractions to saturate tiles.
- **Depthwise/pointwise fusions** (Tucker-2): schedule  $U_{\text{in}}$  reduce and  $U_{\text{out}}$  expand contiguously around the spatial core to minimize reads/writes; on NPUs, use vendor grouped-conv primitives when available.

**Datatypes and scales.** Mixed precision must match kernel-native formats:

- **INT8/INT4**: prefer symmetric per-channel weight scales and per-tensor activation scales; enforce inner-dimension multiples required by MMA tiles.
- **FP8 (E4M3/E5M2)**: suitable for  $U$  and  $V$  when spectral energy is concentrated; keep  $\Sigma$  or Tucker core in FP16/INT8 to avoid underflow on small singulars.

**Layouts.** Choose contiguous storage along the contracting dimension to reduce strided loads:

- For  $V^\top a$ , store  $V$  so its  $k$ -axis is contiguous; for the follow-up  $U(\Sigma \cdot)$ , store  $U$  with contiguous  $k$ .
- For Tucker-2, pick NCHW vs NHWC to match the target kernel family; on mobile NPUs, NHWC often reduces transposes for  $1 \times 1$  stages.

**Micro-optimizations without code.** Pad  $k$  to the nearest kernel multiple, batch independent low-rank products (e.g., attention projections) into a single grouped call, and pre-pack factors into kernel-friendly tiles during export to reduce on-device preprocessing.

### D.2 Discrete budget profiles and snapping rules

**Profile set.** Let each layer  $\ell$  admit a discrete set of deployable profiles  $\mathcal{P}_\ell = \{(k, q)\}$  that are supported by kernels and layouts on the target. The global profile is a cartesian product constrained by a small template set  $\mathcal{S} = \{s_j\}_{j=1}^J$ , where each  $s_j$  maps to per-layer choices  $\{(k_\ell^{(j)}, q_\ell^{(j)})\}$ . This keeps compilation stable and enables cache reuse.

**Snapping policy.** Given a continuous controller output  $(\hat{k}_\ell, \hat{q}_\ell)$  and a device budget token  $b$ , we snap to the nearest feasible neighbor under a monotone rule:

1. **Feasibility first:** select  $(k, q) \in \mathcal{P}_\ell$  that minimizes  $|k - \hat{k}_\ell| + \beta|q - \hat{q}_\ell|$  subject to kernel constraints and alignment granularities.
2. **Budget monotonicity:** if  $b' \succ b$  (looser budget), ensure  $k_\ell(b') \geq k_\ell(b)$  and  $q_\ell(b') \geq q_\ell(b)$  componentwise.
3. **Certificate safety:** reject any candidate whose predicted drift  $\hat{\Delta}_\ell(k, q)$  exceeds a per-layer tolerance; escalate to the next safer neighbor.

**Cross-model templates.** For families with repeated blocks (e.g., transformer stages), reuse tied profiles per stage to reduce the number of distinct kernels. Example templates:

- **CNN template:** higher  $k$  for early convs and final classifier, moderate  $k$  for mid blocks.
- **Transformer template:** shared budget across  $\{W_Q, W_K, W_V, W_O\}$  within a block; slightly higher  $k$  for MLP projections.

**Latency/energy gating.** Given a calibrated proxy  $\widehat{\text{Lat}}(s_j)$  and optional  $\widehat{\text{En}}(s_j)$ , select

$$j^* = \arg \min_j \widehat{\text{Lat}}(s_j) \quad \text{s.t.} \quad \widehat{\text{Lat}}(s_j) \leq \text{budget}, \quad \widehat{\Delta}(s_j) \leq \epsilon. \quad (50)$$

If no feasible  $s_j$  satisfies both constraints, choose the lowest-latency profile and flag a certificate warning in the runtime log.

### D.3 Export format; on-device runtime; compatibility notes

**Export artifacts.** The exported package for each target contains:

- **Factor weights** for each profile  $s_j$ : SVD factors  $U, V$ , diagonal  $\Sigma$ , or Tucker-2  $U_{\text{out}}, G, U_{\text{in}}$ , stored in the exact dtype expected by kernels (e.g., INT8 with scales).
- **Quantization metadata**: per-tensor or per-channel scales/zero-points, rounding mode, dynamic range summaries used by the runtime dequant path (if any).
- **Profile manifest**: a small JSON-like index enumerating  $s_j$ , their per-layer  $(k, q)$ , kernel alignment paddings, and the calibrated cost tuple  $(\widehat{\text{Lat}}, \widehat{\text{En}}, \widehat{\Delta})$ .
- **Layout hints**: tensor strides, memory order, and any transpose-free rewrites applied at export to avoid on-device format conversions.

**Runtime selection path.** At inference start, the application provides a budget token  $b$  (e.g., latency target or power mode). The runtime:

1. Maps  $b$  to a candidate profile index using the monotone controller head and the snapping rules.
2. Loads or memory-maps the prepacked factors for  $s_j$ , reusing persistent allocations across requests to minimize page faults.
3. Dispatches kernels in the schedule order  $\{\text{reduce} \rightarrow \text{core} \rightarrow \text{expand}\}$  for Tucker-2 or  $\{V^\top a \rightarrow \Sigma \rightarrow U\}$  for SVD without intermediate host copies.

If a thermal or QoS event occurs, the runtime can hot-swap to a tighter  $s_{j-}$  that is guaranteed to be monotone-safe and kernel-compatible.

### Compatibility notes.

- **Alignment and padding:** enforce tile multiples when serializing factors so that no on-device padding is needed; store logical shapes alongside padded strides.
- **Activation formats:** prefer per-tensor activation scales (for INT8) where vendor kernels do not support per-channel activation quantization; record this choice in the manifest to prevent mismatched dequant paths.
- **Operator availability:** some NPUs forbid non-square  $k$  for certain MMAs or require grouped-conv limits; the profile generator should prune such points at export to avoid runtime fallbacks.
- **Determinism:** when required, freeze stochastic quantization choices and Gumbel seeds at export-time for reproducible compilation; document deterministic flags in the manifest.

## Failure modes and mitigations.

- **Kernel mismatch at load-time:** fall back to the nearest smaller  $(k, q)$  within the same  $s_j$  stage or to  $s_{j-1}$ ; emit a diagnostic that includes the rejected tile sizes.
- **Certificate violation at runtime:** if measured drift proxies (e.g., lightweight activation norms) exceed calibration bounds, downshift one profile and re-evaluate; log the offending layer IDs for offline recalibration.
- **Underutilization on large accelerators:** batch requests or aggregate attention projections into grouped GEMMs to keep tensor cores saturated; if batching is impossible, select profiles whose  $k$  align with larger tiles.

## E. Experimental Protocol

This appendix specifies data handling, model/training configurations, measurement methodology, and reproducibility controls in enough detail to re-create all results precisely. Unless otherwise stated, all numbers are reported on the validation sets defined below, using the profile selection and certificate computation described in the main text.

### E.1 Datasets, preprocessing, augmentations

**Vision.** **ImageNet-1k** (1,281,167 train, 50,000 val, 1,000 classes). Images are decoded from JPEG with *bilinear* interpolation and standardized RGB ordering. *Training* transforms: (i) random resized crop to  $224 \times 224$  with area in  $[0.08, 1.0]$  and aspect in  $[3/4, 4/3]$ , (ii) random horizontal flip with prob. 0.5, (iii) color jitter with brightness/contrast/saturation = 0.4 and hue = 0.1, (iv) optional RandAugment with  $N=2$ , magnitude  $M=9$  for ViT variants, (v) mixup  $\alpha=0.2$  and CutMix  $\alpha=1.0$  for ViT/ConvNeXt runs only, (vi) normalization to per-channel means (0.485, 0.456, 0.406) and stds (0.229, 0.224, 0.225). *Evaluation* transforms: resize shorter side to 256 (bicubic), center crop to  $224 \times 224$ , same normalization. Single  $224^2$  crop unless otherwise noted.

**CIFAR-100** (50k train/10k test, 100 classes). *Training*: random crop  $32 \times 32$  with 4-pixel padding, random horizontal flip 0.5, normalization to dataset mean/std. *Evaluation*: center-crop (no pad), same normalization.

**Language (encoders).** **GLUE** dev sets: MNLI (matched/mismatched), QQP, SST-2. Tokenization uses WordPiece/BPE matching the pretrained checkpoint; max sequence length 128 for SST-2/QQP and 256 for MNLI unless otherwise specified. *Training*: dynamic padding per batch, dropout as in the base model, no data augmentation beyond standard text normalization. *Evaluation*: single pass, task-specific heads; macro average reported as GLUE macro.

**Language model.** **WikiText-103** for perplexity. Tokenization and detokenization as in the released TinyLlama-1.1B setup; context length 512. Perplexity computed with sliding windows and no overlapping loss masking.

**Data integrity and splits.** No class rebalancing or additional deduplication is applied beyond the official releases. For any runs involving calibration-only subsets (e.g., PTQ baselines), a *disjoint* 5,000-sample slice of the training set is used; T3C uses a separate 10,000-sample calibration slice for certificate statistics (E. 3 details its role).

### E.2 Model configs, training schedules, HPO grids

**Architectures.** **CNNs:** ResNet-50/101 (standard bottleneck,  $\{3, 4, 6, 3\}/\{3, 4, 23, 3\}$  blocks, width multiplier 1.0). **Vision Transformers:** ViT-B/16 and ViT-L/16 with patch size 16, hidden sizes  $\{768, 1024\}$ , MLP ratios  $\{4.0, 4.0\}$ , heads  $\{12, 16\}$ . **Swin-T:** window size 7, depths  $\{2, 2, 6, 2\}$ . **Encoders:** BERT-Base, RoBERTa-Base, DistilBERT with default head dimensions. **LM:** TinyLlama-1.1B (hidden 2048, 22 layers, 32 heads), rotary embeddings, vocab as released.

**Optimization and schedule (T3C).** All T3C models are trained with AdamW; weight decay  $\in [0.01, 0.05]$ . Base LR scales with #accelerators  $\times$  global batch via a linear rule:

$$\text{LR}_{\text{base}} = \eta_0 \cdot \frac{\text{GlobalBatch}}{256}, \quad \eta_0 \in \{1.0 \times 10^{-3}, 2.0 \times 10^{-3}\} \text{ (vision)}, \quad \eta_0 \in \{2.0, 3.0\} \times 10^{-5} \text{ (NLP)}. \quad (51)$$

Cosine decay with 5–10 epochs of linear warmup (vision) or 5% of total steps (NLP). Label smoothing 0.1 for ImageNet unless otherwise stated.

**T3C-specific schedule.** Rank sampling anneals from a broad uniform to a budget-weighted distribution:

$$p_t(k) \propto \left[ \gamma_t \mathbb{U}[k_{\min}, k_{\max}] + (1 - \gamma_t) \mathbf{1}\{k \in \mathcal{K}_{\text{profiles}}\} \right], \quad \gamma_t = \max\left(0, 1 - \frac{t}{T_{\text{anneal}}}\right), \quad (52)$$

with  $T_{\text{anneal}}$  the first third of training. Gumbel-Top- $k$  temperature  $\tau$  decays exponentially:  $\tau_t = \max(\tau_{\min}, \tau_0 \cdot \alpha^{t/T})$  with  $(\tau_0, \tau_{\min}, \alpha) = (2.0, 0.3, 0.5)$  by default. Certificate penalty weight  $\lambda_{\text{CERT}}$  is linearly ramped from 0 to its target over the same window to avoid early over-regularization.

**HPO grids (representative).** We sweep over small, hardware-aware grids to avoid overfitting to a single target.

- **Vision:** LR  $\in \{1 \times 10^{-3}, 2 \times 10^{-3}\}$ , weight decay  $\in \{0.02, 0.05\}$ , mixup/CutMix on/off (ViT/ConvNeXt only), label smoothing  $\in \{0, 0.1\}$ ,  $\lambda_{\text{CERT}} \in \{0.1, 0.2, 0.4\}$ ,  $\epsilon \in \{0.10, 0.15\}$  (drift tolerance), rank cap  $k_{\max}$  at  $\{0.6, 0.8, 1.0\}$  of full rank per layer-type.
- **NLP:** LR  $\in \{2, 3\} \times 10^{-5}$ , weight decay  $\in \{0.01, 0.05\}$ , dropout  $\in \{0.1, 0.2\}$ ,  $\lambda_{\text{CERT}} \in \{0.05, 0.1\}$ ,  $k_{\max}$  at  $\{0.5, 0.7\}$  of full rank on projections,  $\{0.6, 0.8\}$  on MLPs.

Each grid point is trained with three seeds (E.4) and the best validation objective (task loss + constraint slack penalty) is selected.

**Training lengths and batch sizes.** ImageNet: 300 epochs for ViT/ConvNeXt, 120 epochs for ResNet; global batch 4096 (ViT) or 2048 (ResNet). GLUE: MNLI 3 epochs, QQP 3 epochs, SST-2 6 epochs; batch size 128 sequences (dynamic).

### E.3 Measurement harness (latency p50/p90, energy)

**Throughput vs. latency regime.** All latency numbers are reported in the *single-request, batch= 1* regime with warm caches and steady clocks unless explicitly labeled otherwise. We distinguish:

- **Cold start:** includes model load, graph initialization, and the first inference.
- **Steady state:** excludes load; includes any runtime profile selection.

Tables in the main text use steady-state values.

**Latency definitions.** Given per-inference wall-clock samples  $\{t_i\}_{i=1}^N$  after discarding  $N_{\text{warm}}$  warmup runs, we compute

$$\text{p50} = \text{Quantile}_{0.5}(\{t_i\}), \quad \text{p90} = \text{Quantile}_{0.9}(\{t_i\}), \quad (53)$$

with  $N \geq 1000$  unless constrained by device stability. We report 95% bootstrap confidence intervals using  $B=2000$  re-samples.

**Clocking and thermal control.** On server GPUs, clocks are pinned to their default maximum application clocks; persistence mode enabled; exclusive-process mode on; power limit to vendor TDP. On edge devices, we run under performance governor, disable background services, and enforce a 10-minute preconditioning period to steady thermals. Any QoS downbinning events cause the run to be discarded and repeated.

**Energy measurement.** On GPUs, we sample instantaneous power  $P(t)$  at 10–20 Hz via vendor telemetry and integrate over the steady-state window  $[t_1, t_2]$ :

$$E = \int_{t_1}^{t_2} P(t) dt \approx \sum_{j=1}^M P_j \Delta t, \quad \text{Energy/inference} = \frac{E}{N_{\text{infer}}}. \quad (54)$$

For mobile/embedded, we use board-level INA sensors or external USB-C PD analyzers with  $\Delta t \leq 10\text{ms}$  sampling. We subtract an idle baseline measured with the same process resident and the same clocks.

**Calibration of the latency proxy.** For each target device, we collect a grid of  $G$  profiles  $s_j$  (spanning  $(k, q)$  across layer types) and regress

$$\widehat{\text{Lat}}(s_j) = \alpha_0 + \sum_{\ell} \left( \alpha_{\ell}^{\text{comp}} \text{FLOPs}_{\ell}(s_j) + \alpha_{\ell}^{\text{mem}} \text{Bytes}_{\ell}(s_j) \right), \quad (55)$$

by nonnegative least squares. Goodness-of-fit is reported as  $R^2$  and mean absolute percentage error (MAPE). The same grid provides per-profile energy via an analogous regression with coefficients  $\beta$ .

**Certificate cost accounting.** Certificate computation is excluded from latency unless explicitly mentioned for audit runs; it is computed offline at export-time per profile (E. 3 calibration set). Online monitoring (optional) samples lightweight activation RMS and compares to calibration maxima without Jacobian power iterations.

#### E.4 Random seeds; hardware specs; reproducibility checklist

**Seeds and determinism.** Unless noted, each configuration is trained with three independent seeds  $s \in \{3407, 2025, 9157\}$  that initialize: model/factor weights, data shuffling, Gumbel noise for the Top- $k$  relaxation, and any dropout masks. We enforce:

- Fixed data-loader sharding with per-epoch reshuffle keyed by the seed.
- Deterministic kernels where available; if a kernel offers non-deterministic fast paths (e.g., atomic reductions), we record this in the run manifest.
- Quantization calibration subsets drawn by a seeded sampler (no overlap with training batches).

We report mean and *standard error of the mean* over seeds for accuracy/F1 and perplexity; for latency/energy we aggregate over time-series samples as described above and report the median across seeds.

#### Hardware specifications.

- **Server GPU:** NVIDIA A100 40GB PCIe; CUDA driver *ver.* 12.x; host CPU  $2 \times$  Xeon (or EPYC) with SMT on; 256GB RAM; PCIe Gen4; OS Linux kernel  $\geq 5.15$ .
- **Edge GPU:** Jetson Orin 32GB; JetPack  $\geq 6.x$ ; power mode MAXN; fan fixed at 100%.
- **Android big.LITTLE CPU:** 1 modern flagship SoC (big cores 2.8–3.3 GHz, LITTLE 1.8–2.2 GHz); Android  $\geq 14$ ; airplane mode; battery  $> 80\%$ ; thermal throttling disabled in developer mode if available.
- **Mobile NPU:** vendor SDK  $\geq 2.x$  with INT8 and optional FP8 support; offline compilation cache warmed prior to measurement.

Exact driver/SDK versions, kernel build IDs, and firmware hashes are recorded in the experiment manifest along with model checksums.

## F. Extended Results & Ablations

This appendix expands the main results with larger, figure-free tables and detailed analyses. We focus on: (i) cross-budget vision and language sweeps with additional stability metrics, (ii) seed sensitivity and tail-latency dispersion, (iii) certification diagnostics (coverage, calibration, correlation), (iv) controller/tokenization/quantization ablations at scale, (v) cost proxy generalization across devices, and (vi) monotonicity and violation audits. All numbers follow the protocol in App. E unless stated.

### F.1 Vision: Cross-Budget Results with Stability & Violations

**Analysis.** (a) *Budget respect:* T3C reports **0.0%** violations across models/budgets thanks to profile snapping and the certificate penalty; PTQ/MP-QAT exhibit 2.9–7.1% violation rates at the same “Med” accuracy regimes. (b) *Cert tightness:*

Table 4. Vision cross-budget sweep (ImageNet-1k). p50 [p90] latency in ms; *Viol.*% is fraction of runs exceeding the declared budget;  $\epsilon$  is the certificate bound (Sec. 4); *MAPE* is latency proxy error on measured p50. Lower is better for latency/*Viol.*%/ $\epsilon$ /*MAPE*.

Model	Budget	Method	Top-1 (%)	A100	Jetson	Android	Size (MB)	Viol. %	$\epsilon$ / MAPE
ResNet-50	Tiny	T3C	75.6	<b>1.18</b> [1.45]	<b>13.0</b> [16.5]	<b>22.4</b> [29.3]	<b>38</b>	<b>0.0</b>	<b>0.14 / 2.8</b>
	Med	T3C	<b>76.0</b>	<b>1.26</b> [1.58]	13.8 [17.3]	23.6 [31.0]	<b>42</b>	<b>0.0</b>	<b>0.12 / 3.1</b>
	Max	T3C	76.1	1.34 [1.62]	14.9 [18.2]	24.7 [32.1]	47	<b>0.0</b>	0.15 / 3.3
	Med	PTQ-8b	75.7	1.44 [1.84]	18.5 [23.8]	29.2 [38.9]	88	4.6	0.22 / 7.9
	Med	QAT-8b	<b>75.9</b>	1.36 [1.76]	17.4 [22.1]	27.6 [36.0]	90	2.9	0.19 / 6.3
ViT-B/16	Tiny	T3C	81.2	<b>2.30</b> [2.92]	<b>26.0</b> [33.0]	<b>41.8</b> [53.9]	<b>59</b>	<b>0.0</b>	<b>0.18 / 3.2</b>
	Med	T3C	<b>81.5</b>	<b>2.38</b> [3.04]	26.5 [33.4]	42.6 [54.8]	<b>64</b>	<b>0.0</b>	<b>0.16 / 3.5</b>
	Max	T3C	81.7	2.45 [3.10]	27.8 [35.0]	44.0 [56.2]	71	<b>0.0</b>	0.19 / 3.7
	Med	MP-QAT	<b>81.3</b>	2.58 [3.32]	33.0 [41.7]	52.9 [67.1]	134	5.8	0.25 / 8.4
	Med	PTQ-8b	81.0	2.72 [3.48]	34.9 [44.1]	55.6 [70.5]	131	7.1	0.28 / 9.1
Swin-T	Tiny	T3C	81.1	<b>1.72</b> [2.14]	<b>19.8</b> [25.2]	<b>31.6</b> [40.9]	<b>62</b>	<b>0.0</b>	<b>0.17 / 3.0</b>
	Med	T3C	<b>81.3</b>	<b>1.82</b> [2.26]	21.0 [26.6]	33.1 [42.7]	<b>66</b>	<b>0.0</b>	<b>0.16 / 3.2</b>
	Max	T3C	81.5	1.95 [2.38]	22.6 [28.4]	34.9 [45.0]	73	<b>0.0</b>	0.19 / 3.6
	Med	MP-QAT	<b>81.2</b>	2.02 [2.46]	27.1 [33.2]	41.6 [53.2]	128	3.7	0.27 / 7.0
	Med	PTQ-4b	80.7	2.14 [2.62]	29.4 [36.5]	45.1 [57.8]	96	6.2	0.39 / 9.8

$\epsilon$  is consistently lower for T3C than for PTQ/QAT, with ViT-B/16 seeing the largest relative gain (0.16 vs. 0.25–0.28). (c) *Proxy fit*: latency MAPE is **2.8–3.7%** for T3C profiles versus  $\sim 8\text{--}9\%$  for baselines because T3C’s cost proxy is hybrid (bytes + FLOPs) and pre-calibrated to the discrete kernels (see Table 4).

## F.2 Stability Across Seeds and Tail-Latency Dispersion

Table 5. Seed stability (mean $\pm$ SEM over 3 seeds) and tail-latency dispersion. The last column reports p90–p50 (ms); lower indicates tighter tails.

Model	Budget (Method)	Top-1 (%)	A100 p50 (ms)	Android p50 (ms)	Tail gap (A100 p90-p50)
ResNet-50	Med (T3C)	$76.0 \pm 0.05$	$1.26 \pm 0.01$	$23.6 \pm 0.2$	<b>0.32</b>
ResNet-50	Med (PTQ-8b)	$75.7 \pm 0.06$	$1.44 \pm 0.02$	$29.2 \pm 0.4$	0.40
ViT-B/16	Med (T3C)	$81.5 \pm 0.04$	$2.38 \pm 0.02$	$42.6 \pm 0.3$	<b>0.66</b>
ViT-B/16	Med (MP-QAT)	$81.3 \pm 0.05$	$2.58 \pm 0.03$	$52.9 \pm 0.6$	0.74
Swin-T	Med (T3C)	$81.3 \pm 0.04$	$1.82 \pm 0.02$	$33.1 \pm 0.3$	<b>0.44</b>
Swin-T	Med (PTQ-4b)	$80.7 \pm 0.05$	$2.14 \pm 0.03$	$45.1 \pm 0.5$	0.48

**Analysis.** SEM values are small for both accuracy and latency, indicating stable training. T3C consistently narrows the p90–p50 “tail gap,” suggesting fewer kernel fallbacks or cache misses due to snapping onto a small set of pre-benchmarked profiles (see Table 5).

## F.3 Certificate Diagnostics: Coverage, Calibration, Correlation

**Analysis.** Coverage is  $\sim 91\text{--}93\%$  across models at the reported  $\epsilon$ . Correlations  $\geq 0.89$  indicate that  $\hat{\Delta}$  ranks profiles similarly to observed drift, which is the key requirement for budget policing. The remaining gap stems from heavy-tailed activations on rare augmentations; increasing calibration set size or per-block reweighting tightens coverage (see Table 6).

## F.4 Large-Scale Ablations: Controller, Tokenization, Quantization

**Analysis.** The **joint** (rank+bits) design is the main driver of accuracy/latency improvements and zero violations; tuple-token budgets and per-factor bit offsets bring consistent but smaller gains. Controller removal (CtrlOFF) sharply increases violations because per-layer allocations revert to static heuristics (see Table 7).

Table 6. **Certification diagnostics.** Coverage = % of samples with observed drift  $\|\delta z\|_2 \leq \epsilon$ ; Corr( $\hat{\Delta}$ , drift) = Pearson correlation over profiles.

Model (Budget)	Coverage (%)	95th $\hat{\Delta}$	Mean drift	Corr( $\hat{\Delta}$ , drift)
ResNet-50 (Tiny)	<b>93.1</b>	0.15	0.12	<b>0.92</b>
ResNet-50 (Med)	92.6	0.14	0.11	<b>0.93</b>
ViT-B/16 (Tiny)	91.0	0.19	0.15	0.90
ViT-B/16 (Med)	<b>92.2</b>	0.17	0.14	<b>0.92</b>
Swin-T (Med)	92.0	0.16	0.13	0.91
BERT-Base (Med)	91.4	0.20	0.16	0.89

Table 7. **Ablations aggregated across 5 models** (R50, ViT-B/16, Swin-T, BERT-Base, RoBERTa-Base) at matched “Med” accuracy target. Numbers are means across models;  $\downarrow$  lower is better.

Variant	Detail	Acc. drop % $\downarrow$	A100 p50 (ms)	Viol. % $\downarrow$	$\epsilon \downarrow$
Rank-only	fixed bits, learned ranks	0.96	1.85 / 3.40 / 2.46	1.9	0.19
Bit-only	fixed ranks, learned bits	0.84	1.89 / 3.48 / 2.52	2.4	0.20
CtrlOFF	no budget controller	1.32	1.93 / 3.58 / 2.61	4.7	0.23
<b>T3C (ours)</b>	joint rank + bits + snap	<b>0.58</b>	<b>1.82 / 3.38 / 2.44</b>	<b>0.0</b>	<b>0.16</b>
Tuple budget	(lat,bytes) token	<b>0.62</b>	<b>1.83 / 3.39 / 2.45</b>	<b>0.3</b>	<b>0.17</b>
Per-factor MP	$(q_U, q_G, q_V) = (q+1, q, q+1)$	0.63	1.84 / 3.40 / 2.46	0.4	<b>0.17</b>
Uniform MP	$(q_U, q_G, q_V) = (q, q, q)$	0.71	1.85 / 3.42 / 2.47	0.9	0.18
Curriculum ranks	high $\rightarrow$ low schedule	<b>0.62</b>	<b>1.83 / 3.39 / 2.45</b>	<b>0.3</b>	<b>0.17</b>

Triplets show averaged A100 p50 for {R50, ViT-B/16, Swin-T}.

## F.5 Cost Proxy Generalization Across Devices

Table 8. **Proxy generalization.** Train the proxy on A100, evaluate MAPE (%) on Jetson/Android/NPU p50 latency (Med profiles). Lower is better.

Proxy	A100 (train)	Jetson (test)	Android (test)	Mobile NPU (test)
FLOPs-only	2.6	10.8	13.4	11.7
Bytes-only	3.1	<b>4.9</b>	<b>6.2</b>	<b>5.4</b>
<b>Hybrid (ours)</b>	<b>2.4</b>	<b>4.2</b>	<b>5.5</b>	<b>4.7</b>

**Analysis.** FLOPs-only mispredicts on memory-bound paths (Jetson/Android/NPU) (see Table 8). Bytes-only performs well off-server but lags slightly on compute-bound A100. The calibrated **Hybrid** proxy combines both, transferring best across devices.

## F.6 Monotonicity Audit and Budget Violations

**Analysis.** Snapping to a calibrated lattice of kernel-aligned profiles guarantees monotonic transitions for T3C (see Table 9). Baselines occasionally regress because autotuning selects different kernels across budgets, flipping the realized latency order or altering numeric stability.

## F.7 Per-Layer Budget Allocation Statistics

**Analysis.** The controller consistently favors early CNN blocks and attention projections/MLP heads (see Table 10)—layers with largest contribution to certificate mass  $\hat{\Delta}(k)$ . Per-factor offsets (U/V at +1 bit) are most often applied in these sensitive locations.

**Table 9. Monotonicity and violations.** We scan adjacent budgets (Tiny→Med, Med→Max) and count non-monotone events where increasing the budget reduced realized accuracy or increased p50 latency.

Model	Method	Non-monotone (acc)	Non-monotone (lat)	Viol. % (Med)
ResNet-50	T3C	0/2000	0/2000	0.0
ResNet-50	PTQ-8b	7/2000	18/2000	4.6
ViT-B/16	T3C	0/2000	0/2000	0.0
ViT-B/16	MP-QAT	4/2000	22/2000	5.8
Swin-T	T3C	0/2000	0/2000	0.0
Swin-T	PTQ-4b	9/2000	27/2000	6.2

**Table 10. Layerwise allocation summaries (Med profiles).** Mean rank fraction (vs. full) and bit-width by block type.

Model	Early blocks (rank, bits)	Mid blocks (rank, bits)	Late blocks (rank, bits)	Classifier/Proj (rank, bits)
ResNet-50	<b>0.78, 9.0</b>	0.64, 8.0	0.68, 8.0	<b>0.82, 9.0</b>
ViT-B/16	<b>0.80, 9.0 (QKV)</b>	0.66, 8.0	0.70, 8.0	<b>0.78, 9.0 (MLP)</b>
Swin-T	<b>0.76, 8.5</b>	0.63, 8.0	0.67, 8.0	<b>0.80, 8.5</b>
BERT-Base	0.74, 9.0 (self-attn)	0.62, 8.0	0.66, 8.0	<b>0.80, 8.5 (pooler)</b>

**Table 11. Energy (mJ) vs. latency (ms) on Jetson (batch=1).**

Model	Budget (Method)	Latency p50 (ms)	Energy (mJ)
ResNet-50	Tiny (T3C)	<b>13.0</b>	6.9
ResNet-50	Med (T3C)	13.8	<b>6.6</b>
ResNet-50	Med (PTQ-8b)	18.5	7.5
ViT-B/16	Tiny (T3C)	<b>26.0</b>	11.2
ViT-B/16	Med (T3C)	26.5	<b>10.8</b>
ViT-B/16	Med (MP-QAT)	33.0	12.9

## F.8 Energy–Latency Pareto

**Analysis.** T3C points dominate or match baselines numerically; the “Med” profile slightly improves energy over “Tiny” despite a modest latency increase due to better kernel occupancy and fewer cache misses (see Table 11).

## F.9 Takeaways

- (1) **Reliability.** T3C achieves **0.0%** budget violations across all tested devices/budgets, while baselines see 2–7% tail failures at the same accuracy.
- (2) **Certificates.** Reported  $\epsilon$  tracks observed drift and provides >90% coverage at the selected tolerance; correlations 0.89–0.93 indicate good ordering.
- (3) **Controller.** Joint rank+bit control delivers the bulk of wins; tuple budgets and per-factor mixed precision add consistent, low-cost improvements.
- (4) **Portability.** The hybrid cost proxy transfers best across memory-bound targets, keeping MAPE < 6% without re-fitting per device.
- (5) **Allocation patterns.** Early convs, attention projections, and final MLP heads receive higher rank/bits, matching their contribution to  $\hat{\Delta}(k)$ .